JOURNAL OF GEOPHYSICAL RESEARCH, VOL. 113, G02009, doi:10.1029/2007JG000426, 2008

A light-driven, one-dimensional dimethylsulfide biogeochemical cycling model for the Sargasso Sea

Dierdre A. Toole,[1] David A. Siegel,[2] and Scott C. Doney[1]

Received 11 February 2007; revised 26 November 2007; accepted 21 December 2007; published 12 April 2008.

[1] We evaluate the extent to which dimethylsulfide (DMS) cycling in an open-ocean environment can be constrained and parameterized utilizing emerging evidence for the significant impacts of solar ultraviolet radiation (UVR) on the marine organic sulfur cycle. Using the Dacey et al. (1998) 1992–1994 Sargasso Sea DMS data set, in conjunction with an offline turbulent mixing model, we develop and optimize a light driven, one-dimensional DMS model for the upper 140 m. The DMS numerical model is primarily diagnostic in that it incorporates observations of bacterial, phytoplankton, physical, and optical quantities concurrently measured as part of the Bermuda Atlantic Time-series Study (BATS) and Bermuda Bio-Optical Project (BBOP) programs. With the exception of sea-to-air ventilation, each of the sulfur cycling terms is explicitly parameterized or altered by the radiation field. Overall, the model shows considerable skill in capturing the salient features of the DMS distribution, specifically the observed DMS summer paradox whereby peak summer DMS concentrations occur coincident with annual minima in phytoplankton pigment biomass and primary production. The dominant processes controlling the upper-ocean DMS concentrations are phytoplankton UVR-induced DMS release superimposed upon more surface oriented processes such as photolysis and sea-to-air ventilation. The results also demonstrate that mixing alone is not enough to parameterize DMS distributions in this environment. It is critical to directly parameterize the seasonal changes in the flux and attenuation of solar radiation in the upper water column to describe the DMS distribution with depth and allow for experimentation under a variety of climate change scenarios.

Citation: Toole, D. A., D. A. Siegel, and S. C. Doney (2008), A light-driven, one-dimensional dimethylsulfide biogeochemical cycling model for the Sargasso Sea, *J. Geophys. Res.*, *113*, G02009, doi:10.1029/2007JG000426.

1. Introduction and Background

[2] Two decades ago, *Charlson et al.* [1987] proposed that phytoplankton and the marine sulfur cycle are linked in a negative climate feedback loop that has the potential to damp both naturally and anthropogenically induced global temperature perturbations. Once ventilated to the atmosphere, the degradation products of volatile reduced organic sulfur species potentially exert considerable control on the global climate via alterations in radiative properties, acid-base chemistry, halogen cycles, and aerosol iron availability [e.g., *Charlson et al.*, 1987; *Andreae and Crutzen*, 1997; *Ayers and Gillett*, 2000; *Jones et al.*, 2001; *Johansen and Key*, 2006]. Marine biogenic production of dimethylsulfide (DMS) is one of the most important sources of non-sea-salt atmospheric sulfur, representing >90% of the oceanic flux. While studies have observed strong relationships between DMS flux and atmospheric properties such as cloud condensation nuclei concentrations in certain regions [e.g., *Ayers et al.*, 1991; *Ayers and Gras*, 1991; *Vallina et al.*, 2006], evidence confirming a DMS-climate feedback remains elusive.

[3] While the phytoplanktonic synthesis of DMS and its chemical precursor, dimethylsulfoniopropionate (DMSP), are at the core of this climate regulation mechanism, over the years it has become increasingly clear that DMS concentrations and flux to the atmosphere are the result of interactions that span the entire foodweb, including physical and chemical cycling mechanisms [e.g., *Stefels et al.*, 2007]. DMS is derived from bacterial- and phytoplankton- mediated enzymatic cleavage of DMSP, which is synthesized intracellularly by marine phytoplankton at species-dependent concentrations (Figure 1) [*Keller et al.*, 1989; *Andreae and Crutzen*, 1997]. The physiological function of DMSP remains much debated, with suggested roles varying widely including osmotic regulation, chemical defense against grazers, cryoprotection, and internal antioxidant regulation [see *Simó et al.*, 2002, and references therein]. DMS is exuded directly by phytoplankton, with species composition and physiological state and degree of environmental stress influencing the rate of emission [e.g., *La Roche et al.*, 1999]. DMS is also produced through bacterial transforma-

[1] Marine Chemistry and Geochemistry Department, Woods Hole Oceanographic Institution, Woods Hole, Massachusetts, USA.
[2] Institute for Computational Earth System Science, University of California, Santa Barbara, Santa Barbara, California, USA.

0148-0227/08/2007JG000426$09.00

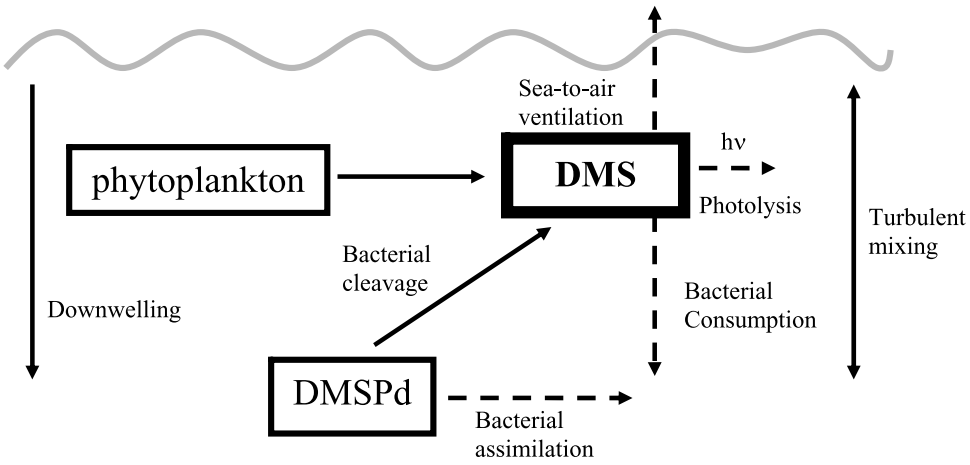

Figure 1. Structure of the DMS biogeochemical cycling model. DMS production processes consist of release from phytoplankton (implicitly via zooplankton grazing, cell senescence, viral lysis, and direct release) and bacterial conversion of DMSPd to yield DMS (solid arrows). Direct and indirect loss processes consist of DMS photolysis, bacterial consumption, atmospheric ventilation, and bacterial DMSPd assimilation (dashed arrows). Physical processes include downwelling and diffusive turbulent mixing. DMSPd concentration is prescribed at 1 nM.

tion of extracellular DMSP that has entered the water column via phytoplankton cell lysis [*Kiene and Service*, 1991; *Ledyard and Dacey*, 1996] and zooplankton grazing [e.g., *Dacey and Wakeham*, 1986]. DMS is removed from the water column primarily through heterotrophic bacterial and phytoplankton consumption, photolysis, and ventilation to the atmosphere [*Kiene and Bates*, 1990; *Simó*, 2001; *Toole et al.*, 2003; *Vila-Costa et al.*, 2006a].

[4] A variety of efforts are ongoing to develop predictive relationships for modeling surface DMS inventories. While the potential for estimating DMS concentrations from satellite ocean color imagery or other global metrics is still under active debate, it is clear from the poor correlations observed between DMS, particulate and dissolved DMSP (DMSPp and DMSPd respectively), and chlorophyll in a variety of field campaigns [e.g., *Kettle et al.*, 1999] that a simple scaling with surface chlorophyll has limited skill in predicting DMS concentrations. A variety of empirical models have been introduced to parameterize DMS concentrations in terms of SeaWiFS-derived surface chlorophyll and Levitus mixed layer depth [*Simó and Dachs*, 2002], a semiempirical relationship for community structure [*Aumont et al.*, 2002; *Belviso et al.*, 2004b], and climatological nutrients and mean daily shortwave radiation [*Anderson et al.*, 2001]. While these models all demonstrate varying degrees of success in certain geographic regions, a review by *Belviso et al.* [2004a] indicates that empirical DMS models show considerable disagreement at subtropical latitudes (20°–40°) and the poles with respect to the magnitude and existence of seasonal variability. Several prognostic biogeochemical models have also been developed that include explicit, dynamic representations of DMS and DMSP production and cycling [e.g., *Gabric et al.*, 1993, 2003; *Archer et al.*, 2002; *Lefevre et al.*, 2002; *Cropp et al.*, 2004; *Le Clainche et al.*, 2004]. While these DMS models do demonstrate considerable increases in predictive skill, none of them explicitly incorporate emerging evidence for the impacts of ultraviolet radiation (UVR, 280–400 nm) on DMS and DMSP biogeochemical cycling processes.

[5] DMSP and its oxidation products (including DMS) have been shown to be highly effective scavengers of reactive oxygen species. The *Sunda et al.* [2002] antioxidant hypothesis suggests that phytoplankton synthesize DMSP, which is converted intracellularly to DMS, as a method to cope with high levels of oxidative stress resulting from UVR exposure as well as metal toxicity and low nutrient concentrations. Several field and laboratory studies have produced mixed results demonstrating that UVR and visible light exposure, mixed layer depth, and stratification alter net community DMS production and intracellular phytoplankton DMS and DMSP production [e.g., *Simó and Pedrós-Alió*, 1999a; *Sunda et al.*, 2002; *Slezak and Herndl*, 2003; *Toole and Siegel*, 2004; *Toole et al.*, 2006; *Vallina and Simó*, 2007]. UVR can also substantially inhibit biological DMS and DMSPd consumption [e.g., *Slezak et al.*, 2001; *Slezak and Herndl*, 2003; *Toole et al.*, 2006], and DMS photochemical loss is directly proportional to UVR [e.g., *Hatton*, 2002; *Toole et al.*, 2003]. Supporting UVR as a modulating factor for DMS distributions, *Toole and Siegel* [2004] demonstrated that >77% of the variability in mixed layer DMS concentrations at the Bermuda Atlantic Time-series Study (BATS) site can be explained in terms of daily UVR dose. Two recent empirical models developed by *Simó and Dachs* [2002] and *Vallina and Simó* [2007] model surface DMS distributions in open-ocean regions as a function of the natural log of mixed layer depth and solar radiance dose respectively. These models have proven to be highly versatile globally in predicting surface DMS concentrations and adequately capture the seasonal cycle at the BATS site. *Lefèvre et al.* [2002] modeled the seasonal DMS and DMSP cycle at BATS using a 1-D ecosystem based model. While they were not able to successfully simulate the large subsurface DMS peak, they achieved the best fit when several model parameters, including the internal

phytoplankton sulfur to nitrogen quota, were scaled by surface visible light intensity. *Vallina et al.* [2008] also uses broad band solar radiation as a proxy for UVR in a dynamic model of DMS which couples sulfur cycling to an established ecological model to assess the principle processes driving the DMS summer paradox. To date however, no attempt has been made to explicitly incorporate the effects of UVR exposure in one-dimensional DMS and DMSP numerical models.

[6] The current decreased stratospheric ozone concentrations, as well as the shoaling of the mixed layer depth predicted under enhanced greenhouse conditions [e.g., *Boyd and Doney*, 2002], suggest it is critical to understand how DMS and DMSP biogeochemical cycling rates will change in response to altered UV fluxes. The objectives of this work are to (1) explore the extent to which the DMS seasonal cycle in an open-ocean environment can be constrained and parameterized utilizing measured biological, chemical, physical, and optical quantities in conjunction with prognostic production and loss processes, (2) elucidate and quantify the importance of the various sulfur biogeochemical cycling pathways, and (3) assess the sensitivity of each process to seasonal changes in UV and visible solar radiation fluxes and attenuation. As the direct and indirect effects of UV and visible radiative forcing are ubiquitous within marine biogeochemical cycles and are expected to be especially strong in open-ocean, oligotrophic regions such as the Sargasso Sea, we use the *Dacey et al.* [1998] 1992–1994 DMS time series for model development, calibration, and optimization. As a final step a sensitivity analysis was carried out to assess the principal processes controlling the concentrations of DMS, suggesting directions for future research.

2. Measurements

2.1. Study Site

[7] The BATS site (31°40′N, 64°10′W) is located in the Northern Sargasso Sea, approximately 85 km southeast of the island of Bermuda. This region is the site of numerous ongoing research projects in which the basic seasonal hydrography, biogeochemistry, and optics have been well characterized and documented [e.g., *Siegel et al.*, 2001; *Steinberg et al.*, 2001]. Summertime is characterized by a strongly stratified, oligotrophic water column with shallow mixed layers marked by high sea surface temperatures (~28–29°C) and relatively low salinity (~36.5 psu) (Figure 2). In the fall and winter, mixed layer depths progressively deepen via convective overturning to depths in excess of 150 m, yielding a relatively homogeneous water column characterized by lower temperatures (~19–20°C) and slightly elevated salinity (~36.6 psu). This deep mixing results in entrainment of nutrients from depth that, in conjunction with the onset of warming and stratification in the spring, drive the variable strength phytoplankton bloom [e.g., *Steinberg et al.*, 2001]. With the exception of these deep mixing periods and eddy pumping events [*McGillicuddy et al.*, 1998] however, nitrate levels in the euphotic zone remain below the limit of detectability by standard techniques. Chlorophyll concentrations peak in the spring coincident with the bloom, are minimum in the surface layers in the summer (<0.05 mg m^{-3}), and exhibit a deep maximum at ~80–100 m in the summer (Figure 3).

[8] The Bermuda Bio-Optical Project provides a concurrently sampled data set (±4 days) of optical properties collected at the BATS site that can also be leveraged for this effort [*Siegel et al.*, 1995, 2001]. Not surprisingly, surface solar fluxes of visible (400–700 nm) and UVR peak in the summer. Chromophoric dissolved organic material absorption coefficients ($a_{CDOM}(\lambda)$) are lowest in the summer in the mixed layer when stratification and UVR dose are greatest and photo-bleaching results (see Table 1 for all symbols). CDOM absorption coefficients are highest in the seasonal thermocline (~60–80 m) in the summer due to local production processes and are fairly homogeneous with depth in the winter due to physical mixing processes, low biological activity, and low UVR fluxes [*Siegel and Michaels*, 1996; *Nelson et al.*, 1998]. Diffuse spectral light attenuation coefficients ($K_d(\lambda)$) are at a minimum in the summer due to the optical clarity of the water column resulting from the combined effects of low $a_{CDOM}(\lambda)$ and chlorophyll. While these patterns are fairly regular in their seasonal progression, this region is characterized by a high degree of interannual variability due to variations in the strength and persistence of wind stress, heat flux, horizontal advection, and the advection of mesoscale features such as eddies [e.g., *Doney*, 1996].

2.2. DMS Time Series

[9] The *Dacey et al.* [1998] 1992–1994 organic sulfur time series consists of twice monthly sampling of DMS, DMSPp, and DMSPd in the upper 140 m at Hydrostation S (32° 10′N, 64° 30′W, ~35 km SE of Bermuda). DMS concentrations exhibit a clear seasonal cycle ranging from a relatively homogenous profile of less than 1 μmol m^{-3} in the winter to concentrations greater than 7 μmol m^{-3} at midwater depths (~25–40 m) associated with high stratification and shoaling of the mixed layer in summer. This observed time and depth variability is a clear example of the so-called 'DMS summer paradox' [*Simó and Pedrós-Alió*, 1999a]. The essence of the paradox is that DMS stocks reach their maximum in July and August, more than two months later than the maximum for its precursor, DMSP, coincident with seasonal minima in phytoplankton pigment biomass and primary production. Although characterized by interannual variability, DMS stocks display a regular seasonal progression which has been shown to be decoupled from the seasonal patterns of particulate and dissolved DMSP [*Dacey et al.*, 1998]. Correlations between DMS and standard in situ properties measured as part of the BATS core sampling program indicate that DMS is in fact regulated most strongly by physical and optical quantities, such as the availability and spectral quality of the underwater light flux [*Toole and Siegel*, 2004].

3. Model Description and Specification

[10] The primary goal of this study is to construct and optimize a simple biogeochemical model to capture the upper-ocean DMS seasonal cycle relying on as many concurrently measured quantities as possible. With this goal in mind, a one-dimensional numerical model of DMS cycling, consistent with the recently proposed antioxidant

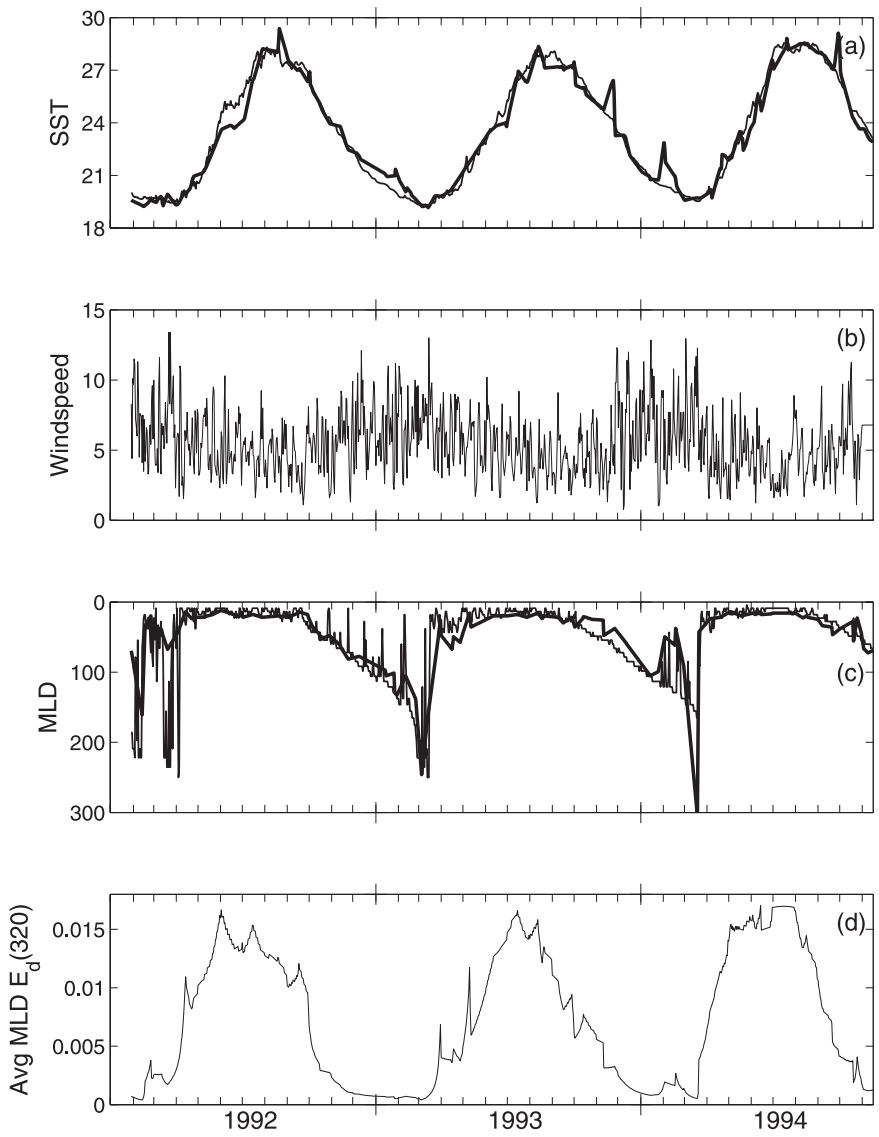

Figure 2. Forcing parameters and results from the KPP physical model (a) sea surface temperature (SST, °C), (b) wind speed (m s^{-1}), (c) mixed layer depth (MLD, m), and (d) mean 320 nm downwelling irradiance dose (E_d(320)) in the mixed layer (W m^{-2}). In Figures 2a and 2c the thick line represents CTD hydrocast data pooled from the BATS and Hydrostation S sites interpolated daily, and the thin line represents results derived from model simulations. Mixed layer depth in Figure 2c was calculated based on a potential density difference of 0.02 kg m^{-3} from the surface.

physiological role for DMS and DMSP [*Sunda et al.*, 2002], was developed. The rate processes consist of physical (turbulent diffusive mixing, downwelling), chemical (photolysis), and biological (bacterial consumption, bacterial production, and phytoplankton release) cycling. The depth- and time-dependent changes in DMS were thus modeled as a combination of these processes:

$$\frac{\partial[DMS]}{\partial t} = \frac{\partial}{\partial z}\left(K_z \frac{\partial[DMS]}{\partial z} - w[DMS]\right) - k_{photo}[DMS] - k_{bac}[DMS] + J_{bac} + J_{phyto} \quad (1)$$

where [*DMS*] is the in situ concentration of DMS (μmol m^{-3}), K_z is vertical diffusivity, w is the net downwelling vertical velocity, k_{photo} and k_{bac} are the first order rate constants for DMS photolysis and bacterial consumption (d^{-1}) respectively, J_{bac} is the bacterial production of DMS from DMSPd consumption (μmol m^{-3} d^{-1}), and J_{phyto} is the DMS release from phytoplankton (μmol m^{-3} d^{-1}) (see Figure 1). Sea-to-air ventilation of DMS is also included as a surface boundary condition. Each of the primary sulfur cycling terms is explicitly parameterized or altered by the radiation field (see below).

[11] Because the goal of this study was to diagnose DMS cycling, DMSP concentrations were not tracked explicitly, although consumption rates were constrained to literature values observed in open-ocean environments. Additionally, the sulfur model is not embedded in an ecosystem model. There are a host of complex biological processes and interactions, including direct exudation, cell senescence,

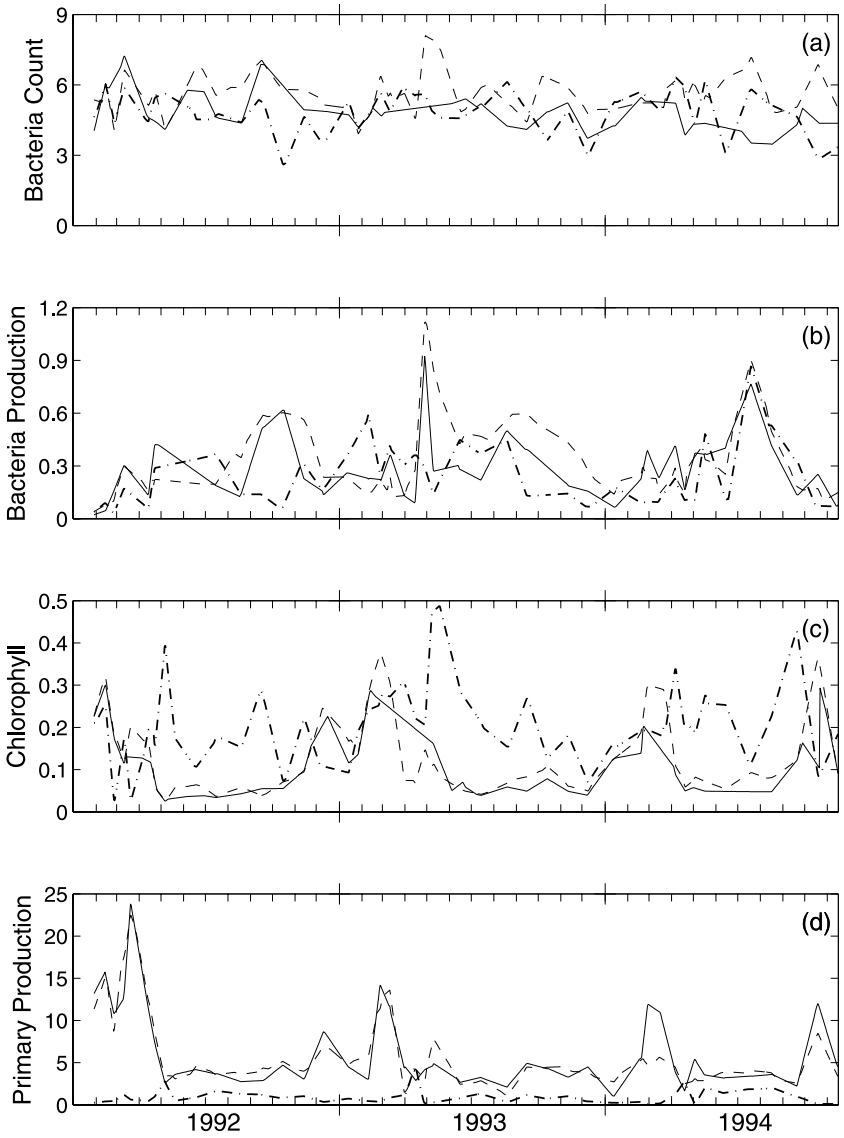

Figure 3. Biological inputs used for model parameterization and forcing derived from the BATS site [*Steinberg et al.*, 2001]: (a) bacterial count (10^8 cells m^{-3}), (b) bacterial productivity (mg C m^{-3} d^{-1}), (c) chlorophyll (mg m^{-3}), and (d) primary productivity (mg C m^{-3} d^{-1}). In all panels the solid line corresponds to the surface, the dashed line is 25 m, and the dash-dot line is 100 m.

zooplankton grazing, and viral lysis, that may impact and regulate the amount of DMS released by phytoplankton that are not resolved in this model. For most of these processes however, the mechanisms and rates are extremely poorly constrained and thus caution must be taken when increasing the complexity of a model to incorporate them. This model directly simulates the amount of DMS that must be released by phytoplankton to balance the chemical, physical, and bacterial DMS cycling processes. As a result, variations in each phytoplankton process (e.g., exudation, grazing, lysis) will not be modeled separately, but will be incorporated into two light-driven production terms (section 3.5). This limits our ability to attribute the modeled patterns to individual phytoplankton processes, but it does allow for an assessment of whether the phytoplankton production rate is directly related to light. A secondary goal of this work is to minimize the number of tunable free parameters because of the scarcity of available rate data for comparison. As mentioned above, concurrently sampled data from the BATS and Bermuda Bio-Optical Project (BBOP) time series field sampling programs were used whenever possible [*Steinberg et al.*, 2001] including wind speed, bacterial cell count, bacterial production, chlorophyll pigment derived biomass, and primary production (Figures 2 and 3 and Table 1).

3.1. Water Column Ultraviolet and Visible Radiation

[12] Wavelength resolved surface incident solar radiation ($E_d(0^+,\lambda)$) was derived from integrated solar radiation

Table 1. Symbols, Sources, and Units for Time Series Measurements From the BATS and BBOP Projects [*Siegel et al.*, 2001; *Steinberg et al.*, 2001], NCEP Satellite and Reanalysis Data Products [*Doney*, 1996; *Doney et al.*, 1998], and Prescribed Values Used as Model Inputs

Symbol	Quantity	Source	Units	Equations
$E_d(0^+,\lambda)$	Spectral surface incident solar radiation just above the ocean interface	Spectral decomposition of NCEP reanalysis product $E_d(0^+)$	W m^{-2} nm^{-1}	(2)
$E_d(z,\lambda)$	Spectral solar radiation propagated to depth z	Estimated from $K_d(\lambda)$ and $E_d(0^+,\lambda)$, assuming 2% surface reflection	W m^{-2} nm^{-1}	(2)
$K_d(\lambda)$	Spectral downwelling diffuse attenuation coefficient	Estimated from BATS chlorophyll, BBOP remote sensing reflectance, and literature a_{water} [*Pope and Fry*, 1997]	m^{-1}	(2), (3)
$E_o(z,\lambda)$	Spectral scalar irradiance	Estimated from $E_d(z,\lambda)$ assuming a 1.2 conversion factor	W m^{-2} nm^{-1}	(4), (5), (6), (8), (9)
$AQY(\lambda)$	Apparent quantum yield for DMS photolysis	*Toole et al.* [2003]	mol DMS photolyzed (mol photons absorbed)$^{-1}$	(4)
$a_{CDOM}(\lambda)$	Absorption by CDOM	Estimated from BBOP remote sensing reflectance [*Maritorena et al.*, 2002]	m^{-1}	(4)
k_{dark}	Dark bacterial DMS consumption rate	Prescribed – 0.25	d^{-1}	(5)
BP	Bacterial production	BATS time series	mg C m^{-3} d^{-1}	(6)
BC	Bacterial count	BATS time series	10^8 cells m^{-3}	(6)
[DMSPd]	DMSPd concentration	Prescribed – 1	nM	(6)
DMS_{yield}	DMS yield from bacterial DMSPd consumption	Prescribed – 10	%	(6)
CHL	Chlorophyll concentration	BATS time series	mg m^{-3}	(7)
I_k	Saturation irradiance for phytoplankton photosynthesis	Estimated from BATS chlorophyll [*Siegel et al.*, 2001]	Ein m^{-2} d^{-1}	(7), (8)
PAR	Photosynthetically available radiation	Estimated from $E_o(z,\lambda)$ integrated 400–700 nm	Ein m^{-2} d^{-1}	(8)
PP	Primary production	BATS time series	mg C m^{-3} d^{-1}	(8)
$E_{inh}(z)$	Biologically effective exposure over UVR wavelengths	Functional form from *Neale et al.* [1998a, 1998b]	Unitless	(9), (10)
$uv_{index}(z)$	UVR-induced stress index	Functional form from *Neale et al.* [1998a, 1998b]	Unitless	(10), (11)
U_{10}	Wind speed 10 m above the sea surface	NCEP reanalysis	m s^{-1}	(12)
Sc	Schmidt number	*Saltzman et al.* [1993] and BATS temperature	Unitless	(12)

($E_d(0^+)$) from the 1992–1994 6 hour resolved NCEP reanalysis data products for the Bermuda site [*Doney*, 1996] (see Table 1 for symbols). Spectral decomposition was based on an incident spectrum from a subtropical region simulated using the Santa Barbara DISORT Atmospheric Radiative Transfer (SBDART [see *Ricchiazzi et al.*, 1998]). The spectral shape of incident irradiance is relatively invariant to a variety of atmospheric conditions including solar zenith angle, water vapor content, and atmospheric aerosols; therefore we considered it constant throughout the time series [see *Ohlmann et al.*, 1996]. The incident irradiance was propagated through the air-sea interface assuming an average 2% surface reflection [*Austin*, 1974] and average daily values were used as model input.

[13] Once within the water column, depth dependent irradiance was estimated assuming that irradiance is attenuated exponentially with depth as:

$$E_d(z,\lambda) = E_d(0^-,\lambda)e^{-K_d(\lambda)z} \quad (2)$$

where $E_d(z,\lambda)$ represents irradiance (W m^{-2} nm^{-1}) at depth z (m) and wavelength λ (nm), $E_d(0^-,\lambda)$ represents the wavelength resolved irradiance just below the sea surface, and $K_d(\lambda)$ is the spectral downwelling diffuse attenuation coefficient (m^{-1}). For all calculations, UV downward normal irradiance ($E_d(z,\lambda)$) was converted to scalar irradiance $E_o(z,\lambda)$ based on a conversion factor of 1.2, which is a reasonable mean value for the chlorophyll and CDOM concentrations observed at the BATS site. Additionally, scalar irradiance at a given wavelength was converted to photon flux via the factor λ/hc where h is Planck's constant (J s) and c is the speed of light in vacuum (m s^{-1}). Spectral $K_d(\lambda)$'s were reconstructed based on absorption and scattering coefficients as [*Kirk*, 1981]:

$$K_d(\lambda) = \sqrt{a(\lambda)^2 + 0.231a(\lambda)b(\lambda)} \quad (3)$$

where $a(\lambda)$ is the spectral total absorption coefficient (m^{-1}), and $b(\lambda)$ is the spectral total scattering coefficient (m^{-1}). Following the methods of *Toole et al.* [2003], absorption and scattering coefficients were estimated as a function of the depth resolved BATS chlorophyll time series [*Gordon and Morel*, 1983], literature values for absorption by pure water [*Pope and Fry*, 1997], and an empirical absorption parameterization that is a function of $a_{CDOM}(443)$ retrievals from a globally optimized semianalytical inherent optical property ocean color inversion model (GSM01 [*Maritorena et al.*, 2002]). These retrievals were derived from remote sensing reflectance spectra collected concurrently to the DMS and DMSP field samples. In addition, for the DMS photolysis calculations (see section 3.2), $a_{CDOM}(\lambda)$ was derived from daily $a_{CDOM}(443)$ retrievals from GSM01, extrapolated spectrally assuming a globally optimized slope of -0.0206 nm^{-1} [*Maritorena et al.*, 2002]. Estimated CDOM absorption coefficient spectra were assumed con-

Table 2. Optimized Best Fit Parameters

Symbol	Equation	Value	Units	Description
c_1	5	29.3	$m^2\ W^{-1}$	Scaling factor for inhibition of bacterial DMS consumption
c_2	6	12.7	10^8 cells mg C^{-1}	Normalized bacterial carbon production to DMSPd consumption conversion factor
c_3	8	0.0045	μmol DMS (mg C)$^{-1}$	Scaling factor for PAR saturation irradiance overflow mechanism
c_4	9	4.66	unitless	BWF constant
c_5	9	0.034	nm^{-1}	BWF slope
c_6	11	0.77	μmol DMS $m^{-3}\ d^{-1}$	Maximum rate of phytoplankton intracellular DMS release from UVR-induced stress

stant over the time course of one day, consistent with the time scales of photobleaching and production processes [*Nelson et al.*, 1998].

3.2. DMS Photolysis

[14] Because DMS does not absorb radiation at wavelengths greater than 260 nm, photolysis must proceed via a photosensitizer or a transient reactive chemical species [*Brimblecombe and Shooter*, 1986]. Without knowledge of the exact reaction photosensitizers, absorption of light by CDOM is used as a proxy [e.g., *Toole et al.*, 2003; *Bouillon and Miller*, 2004]. Depth dependent DMS photolysis rate constants (k_{photo}(z), d^{-1}) were defined as the product of the photolysis apparent quantum yield ($AQY(\lambda)$, mol DMS photolyzed per mol photons absorbed by the reaction photosensitizer) scaled to the in situ DMS concentration and the energy absorbed by the assumed reaction photosensitizer CDOM:

$$k_{photo}(z) = \int_{280}^{400} AQY(\lambda) a_{CDOM}(z,\lambda) E_o(z,\lambda) \frac{\lambda}{hc} d\lambda \qquad (4)$$

where $k_{photo}(z)$ is the depth dependent photolysis rate constant (d^{-1}), $a_{CDOM}(z,\lambda)$ is the estimated, depth dependent spectral CDOM absorption coefficient (m^{-1}, see section 3.1), and $E_o(z, \lambda)$ is the depth dependent spectral scalar irradiance (W m^{-2} nm^{-1}). While considerable geographic variability has been observed in the apparent quantum yield of DMS photolysis, presumably as a result of the quality of in situ CDOM, availability of reactive oxygen species, and concentration of nitrate, a mean $AQY(\lambda)$ and temperature dependence derived from summertime Sargasso Sea samples was utilized throughout the year [see *Toole et al.*, 2003].

3.3. Bacterial DMS Consumption

[15] While organic sulfur research is in its infancy with respect to understanding how light structures biological sulfur cycling dynamics, there is considerable literature available that can be leveraged for this study concerning the impacts of UVR on carbon-based phytoplankton and bacterial processes. Scores of field campaigns indicate that UV-A (320–400 nm) in the absence of UV-B (280–320 nm) induces photoenzymatic repair of DNA [e.g., *Herndl et al.*, 1993, 1997], while high levels of UV-B are associated with DNA damage [e.g., *Karentz et al.*, 1991; *Huot et al.*, 2000], decreases in primary production [e.g., *Boucher and Prezelin*, 1996; *Neale et al.*, 1998a] and reduction of key cellular functions such as the efficiency of Photosystem II [*Schofield et al.*, 1995]. Evidence for the inhibition of bacterial DMS and DMSPd consumption and the repair processes that occur via exposure to longer wavelengths in the UV-A and visible spectral regions have been observed in the field [e.g., *Slezak et al.*, 2001; *Toole et al.*, 2006; *Slezak et al.*, 2007]. In accordance with the inhibitory role of UV-B, heterotrophic bacterial DMS consumption is parameterized as a first order process [e.g., *Kiene and Service*, 1991] in terms of a dark consumption rate constant, which corresponds to the rate constant at depths below the penetration of UV-B radiation, with inhibition at shallower depths following:

$$k_{bac}(z) = \max[k_{dark}(1 - (c_1 E_o(z, 320)), 0] \qquad (5)$$

where $k_{bac}(z)$ is the first order bacterial DMS consumption rate constant (d^{-1}), k_{dark} is the prescribed dark bacterial DMS consumption rate constant (0.25 d^{-1}), and c_1 is an optimized scaling factor (Table 2) which allows the inhibition term to range from 0 to 1 (with 0 corresponding to no UV-B induced inhibition and 1 indicating complete inhibition of the consumption process). Functionally, maximum inhibition will be observed at the surface, with rate constants exponentially increasing to dark bacterial consumption values in accordance with UV-B attenuation. Bacterial DMS consumption is not parameterized in terms of bacterial abundance or productivity observations because, unlike DMSPd consumption, recent studies suggest that DMS is consumed by specialized methylotrophic bacteria and their relative abundance in the open-ocean is unknown [*Vila-Costa et al.*, 2006b].

3.4. Bacterial DMSPd Consumption and DMS Production

[16] Depending on bacterial sulfur and carbon needs, DMSPd consumption occurs via two independent pathways consisting of a cleavage reaction, which proceeds via bacterial DMSP lyase enzymes yielding DMS and acrylic acid [e.g., *Dacey and Blough*, 1987], and a demethylation and demethiolation pathway in which sulfur is incorporated intracellularly into proteins and amino acids such as methionine and cysteine and does not produce DMS [*Kiene and Linn*, 2000b]. DMSPd concentrations are not explicitly calculated in this model and thus bacterial DMSPd consumption rates are bounded to vary within observed ranges for oligotrophic environments. Admittedly, *Dacey et al.* [1998] does include a concurrently sampled DMSPd data set for model calibration/optimization but it was not used due to sampling and methodological improvements in the intervening years. Recently, *Kiene and Slezak* [2006] outlined a variety of issues associated with 'standard' DMSPd sampling methodologies, including the methods utilized by

Dacey et al. [1998] (large volume filtration). In all cases, *Kiene and Slezak* demonstrated that the commonly applied methods artificially elevated DMSPd concentrations (versus small volume drip filtration or dialysis methods) due to cell rupture, thereby releasing particulate DMSP into the dissolved form. They found that in diverse oceanic waters DMSPd concentrations were always less than 3 nM. This contrasts greatly with the *Dacey et al.* [1998] DMSPd concentrations which range up to as large as 19 nM in the upper 140 m. Ultimately, as the aim of this work is to diagnose DMS biogeochemical cycling, DMSPd concentrations were held constant at 1 nM throughout the model simulations. The *Dacey et al.* [1998] DMSPd concentrations show little seasonality and this lack of a strong seasonal cycle, as well as the low concentrations, are supported by an on-going time series currently being collected at the BATS site (D. A. Toole et al., manuscript in preparation, 2008). To assess the effects of a constant DMSPd concentration several sensitivity runs were carried out using the *Dacey et al.* [1998] DMSPd concentrations as input (section 4.5).

[17] Similar to bacterial DMS consumption, bacterial DMSPd consumption was parameterized in terms of the attenuation of UV-B radiation and a dark, uninhibited consumption rate. In contrast to DMS, which is thought to be consumed by a small group of specialized bacteria, DMSPd is consumed in the Sargasso Sea by an array of diverse bacteria [e.g., *Malmstrom et al.*, 2004]. Therefore, the dark DMSPd consumption rate was parameterized in terms of the bacterial growth rate–the ratio of measured leucine incorporation based bacterial production (*BP*, mg C m^{-3} d^{-1}) to measured bacterial count (*BC*, 10^8 cells m^{-3}) using conversion factors outlined by *Carlson et al.* [1996]. While DMSPd consumption rates reflect the complex balance of bacterial growth rates, physiological status, sulfur demand, and the concentration of labile organic compounds such as DMSPd, significant positive correlations have been observed between bacterial production and DMSPd consumption rates in the field [*Kiene and Linn*, 2000a]. DMS evolving from bacterial DMSPd consumption is described as:

$$J_{bac}(z) = c_2 \frac{BP}{BC}[DMSPd](1 - E_o(z, 320))DMS_{yield} \quad (6)$$

where $J_{bac}(z)$ is the bacterial production of DMS from DMSPd consumption (μmol DMS m^{-3} d^{-1}), c_2 is an optimized scaling factor which converts normalized bacterial carbon production (*BP*/*BC*) to DMSPd consumption rate constants (10^8 cells mg C^{-1}), [*DMSPd*] is the DMSPd concentration (μmol DMSPd m^{-3}), and DMS_{yield} is the yield of DMS from DMSPd consumption (%).

[18] Although the samples for leucine incorporation were incubated in the dark, it is important to note that this parameterization may introduce a degree of noise as the rates may display residual inhibition from exposure to UV-B within the water column. DMS and DMSP consumption rates have been shown to be slow to recover from photoinhibition [*Toole et al.*, 2006; D. Slezak et al., unpublished results] so this is potentially the case. Additionally, although in these simulations the fraction of DMSPd converted to DMS (DMS yield) was fixed at 10%, studies suggest that DMS yield may vary as a function of DMSPd availability, bacterial sulfur demand, and bacterial inhibition ranging from 3–40% [e.g., *Simó and Pedrós-Alió*, 1999a; *Merzouk et al.*, 2006; *Slezak et al.*, 2007]. DMS yields in oligotrophic regions tend to be relatively low (<10%) [e.g., *Slezak et al.*, 2007] but work is necessary to isolate the mechanisms and functionalities of this parameter so it can be modeled more rigorously in future efforts.

3.5. Phytoplankton DMS Production

[19] While little is known about how phytoplankton physiologically cope with various forms of oxidative stress, it is generally considered that they up-regulate antioxidant systems. Phytoplankton DMS production is thus modeled consistent with its recently hypothesized antioxidant role [*Sunda et al.*, 2002] because seasonal phytoplankton community succession or zooplankton mediated responses as the source of the DMS summer paradox are inconsistent with the *Dacey et al.* [1998] time series [*Toole and Siegel*, 2004]. DMSP and its oxidation products (DMS, acrylic acid, DMSO, and MSA) have been shown to be highly effective scavengers of reactive oxygen species (ROS). *Sunda et al.* [2002] observed that under conditions of oxidative stress (high UVR exposure), DMS and DMSP cell volume ratios increased dramatically. *Stefels* [2000] also suggested that when cellular growth is unbalanced due to low nutrient concentrations or high fluxes of photosynthetically available radiation (PAR), phytoplankton require a mechanism by which to discard excess reduced compounds and energy. The synthesis of DMSP is hypothesized as an overflow mechanism for excess reduced sulfur compounds (and excess fixed carbon) when the sulfur influx exceeds the cell's ability to synthesize proteins and amino acids. In the Sargasso Sea, because of consistently low levels of ambient nutrients and absorbing pigment compounds, upper water column phytoplankton can spend a large amount of time above PAR saturation irradiance levels suggesting conditions of unbalanced growth. Modeled net biological DMS production from the *Dacey et al.* [1998] data set displayed the largest positive correlations with optical properties strongly suggesting that these two phenomena may be what is mediating phytoplankton DMS synthesis and release in this region [*Toole and Siegel*, 2004].

[20] Because the suggested physiological role(s) for DMSP have not been completely resolved, basic functional relationships to constrain intracellular DMS and DMSP production and release were drawn from parameterizations in the rich primary production literature. DMS release into the water column is modeled as a function of (1) a PAR saturation overflow index and (2) a UVR mediated stress index, analogous to the inhibition of primary production. We use a different approach than standard primary production calculations, however, in that visible light saturation and UVR photoinhibition processes are modeled, and thus impact DMS production, separately. Time-dependent primary production is often parameterized as the product of a maximum primary production rate and a saturating exponential function of irradiance (production saturates at levels of in situ PAR fluxes (E_o(z,PAR)) above I_k) [e.g., *Cullen et al.*, 1992]. Site specific saturation irradiance values were modeled following *Siegel et al.* [2001]:

$$I_k(t) = -18.8CHL(t) + 7.3 \quad (7)$$

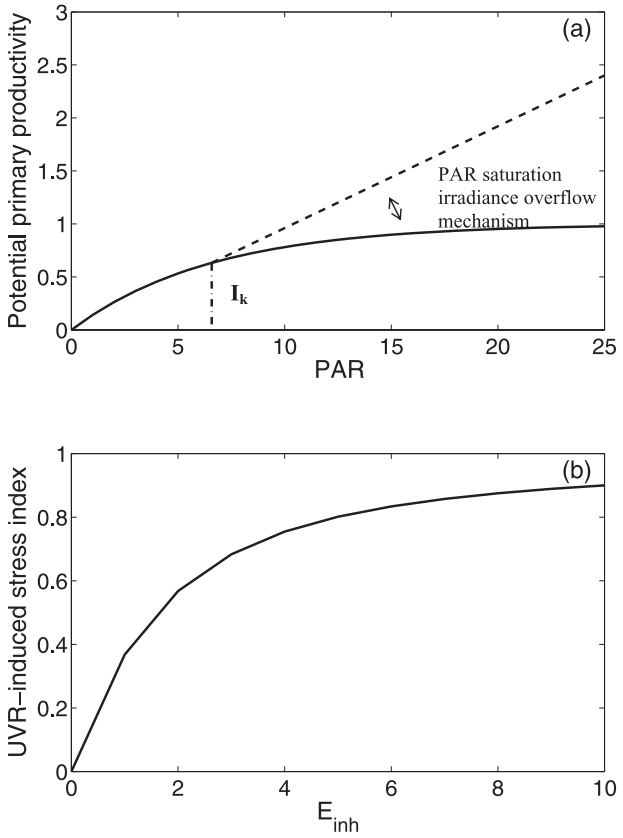

Figure 4. Examples of the phytoplankton DMS release parameterizations for (a) the PAR saturation irradiance overflow mechanism and (b) the UVR-induced stress index. In Figure 4a the solid line represents saturated primary production rates assuming a maximum rate of 1 mg C m^{-3} d^{-1} and a saturation irradiance (I_k) of 6.5 uEin m^{-2} d^{-1}: 1 mg C m^{-3} d^{-1} * $(1 - e^{-(E_o(z,PAR)/I_k)})$, a typical midsummer value for the BATS site [*Siegel et al.*, 1995]. The dashed line represents unsaturated primary production which is calculated as the average slope of the P-E curve for PAR fluxes $\leq I_k$: $(\frac{(1-e^{-1})}{I_k})$, extrapolated linearly to higher PAR fluxes. The amount of DMS release due to excess fixed carbon is parameterized as a function of the difference between the unsaturated rates (dashed line) and the saturated rates (solid line) (equation (8a)). At PAR fluxes below saturation there is no DMS production or release (equation (8b)). In Figure 4b the solid line corresponds to the UVR-induced stress index (equation (9)) calculated over an example range of E_{inh} (equations (9) and (10)).

where I_k is the PAR saturation irradiance (Ein m^{-2} d^{-1}) and CHL is the measured surface chlorophyll concentration (mg m^{-3}). Because we are modeling the synthesis of DMSP as a pool for excess reduced sulfur and fixed carbon under saturating light conditions, as primary production saturates ($E_o(z,PAR) > I_k$), DMSP production will increase proportionally. A critical element of this calculation is that we implicitly assume that a fixed percentage of the synthesized intracellular DMSP is converted to DMS and directly released to the water column each day. Phytoplankton DMSP synthesis (and thus DMS release) due to overflow processes is calculated as the difference between the saturated rates and estimated unsaturated rates extrapolated using the average slope of the P-E curve for fluxes less than I_k (equation (8a) and Figure 4a):

$$J_{phyto-PAR}(z) = c_3 PP(z)\left(\frac{(1-e^{-1})}{I_k}E_o(z,PAR) - \left(1 - e^{-(E_o(z,PAR)/I_k)}\right)\right) \qquad E_{PAR} > I_k \qquad (8a)$$

$$J_{phyto-PAR}(z) = 0 \qquad E_{PAR} \leq I_k \qquad (8b)$$

where $J_{phyto\text{-}PAR}(z)$ is the rate of DMS release into the water column by phytoplankton (μmol DMS m^{-3} d^{-1}) due to unbalanced growth, c_3 is an optimized primary production normalized DMS release rate (μmol DMS mg C^{-1}), and PP is measured primary production (mg C m^{-3} d^{-1}). At PAR fluxes below I_k there is no DMS production or release (equation (8b)).

[21] DMS synthesis is also modeled as a function of a dimensionless, weighted, biologically effective UVR dose analogous to photosynthetic inhibition [e.g., *Neale et al.*, 1998a, 1998b]:

$$E_{inh}(z) = \int_{280}^{400} E_o(z,\lambda)e^{(c_4 - c_5\lambda)}d\lambda \qquad (9)$$

where $E_{inh}(z)$ is the dimensionless biologically effective exposure averaged over the model time-step, c_4 is the biological weighting function (BWF) constant, c_5 is the BWF slope with respect to wavelength of light (nm^{-1}), and the term $e^{(c4-c5\lambda)}$ represents the total BWF following the single exponential slope functional form of *Rundel* [1983] (m^2 W^{-1}). The phytoplanktonic response to the UVR dose was assumed to be inversely proportional to the predicted decrease in photosynthesis [e.g., *Neale et al.*, 1998a] following:

$$uv_{index}(z) = 1 - \frac{1 - e^{-E_{inh}(z)}}{E_{inh}(z)} \qquad (10)$$

where $uv_{index}(z)$ is a dimensionless factor between 0 and 1 that indicates the degree of UVR oxidative stress and thus DMS synthesis (Figure 4b). Biological weighting functions vary based on a variety of factors not treated explicitly in the model including species composition, adaptation to high light environments, nutrient supply, and mixing regime, so the slope and coefficient were optimized during model simulations.

[22] The PAR and UVR DMS production indices were combined to simulate the maximum phytoplankton intracellular DMS release per day:

$$J_{phyto}(z) = J_{phyto-PAR}(z) + c_6 uv_{index}(z) \qquad (11)$$

where $J_{phyto}(z)$ is the total rate of DMS release into the water column by phytoplankton (μmol DMS m^{-3} d^{-1}) and c_6 is the maximum rate of DMS release due to UVR stress (μmol DMS m^{-3} d^{-1}). As mentioned above, while these two light-

driven production indices yield the modeled phytoplankton DMS release per day, there are a variety of additional processes implicit in this rate that can not be resolved with our simple model structure. Variations in the dynamics of the ecosystem structure including zooplankton grazing rates, recycling efficiencies, cell senescence, direct exudation, and viral lysis will not be modeled individually. Given this, the phytoplankton DMS production equations are fundamentally mass balance equations which must balance the loss processes.

3.6. Sea-Air Gas Flux

[23] Sea-to-air DMS flux (μmol m^{-2} d^{-1}) is a surface boundary condition modeled as the product of the DMS concentration in the shallowest grid box and a piston velocity following *Nightingale et al.* [2000]:

$$\text{Flux} = \left(0.22U_{10}^2 + 0.33U_{10}\right)(\text{Sc}/600)^{-0.5}\left([\text{DMS}]_{\text{sfc}} - [\text{DMS}]_{\text{atm}}\right) \quad (12)$$

where U_{10} is the wind speed 10 m above the sea surface (m s^{-1}), $[\text{DMS}]_{\text{sfc}}$ is the concentration of DMS at the sea surface (μmol m^{-3}), $[\text{DMS}]_{\text{atm}}$ is the concentration of DMS in the atmospheric boundary layer (μmol m^{-3}), and Sc is the dimensionless Schmidt number that encapsulates kinematic viscosity and DMS diffusivity. With the exception of very high, sustained wind situations, it is generally considered that $[\text{DMS}]_{\text{atm}}$ is negligible in these calculations [e.g., *McGillis et al.*, 2000]. Sc numbers were modeled as a function of sea surface temperature following *Saltzman et al.* [1993].

3.7. Subtropical Physical Upper-Ocean Model

[24] The physical water column structure was calculated offline using the K-Profile Parameterization (KPP) nonlocal turbulent mixing model of *Large et al.* [1994]. The 1-D model simulates the water column in terms of a surface boundary layer depth and an interior region yielding the depth of the surface mixed layer, and profiles of temperature (T), salinity (S), and vertical diffusivity (K_z). For comparison with observations, mixed layer depths are diagnosed based on the simulated density field. The 1992–1994 6-hour resolved BATS wind stress, wind speed, daily solar radiation, net longwave radiation, and latent and sensible heat flux were incorporated as input from the NCEP reanalysis and satellite data products for the Bermuda site following standard bulk formulae as in *Doney* [1996] and *Doney et al.* [1998]. In addition to turbulent diffusive mixing, because Ekman convergence causes a net downwelling velocity at Bermuda, a downwelling term was added that is zero at the surface, increases linearly to a maximum downward velocity at 30 m, and then decrease linearly to zero again at 250 m [see *Doney et al.*, 1996]. Conservation of mass was maintained by assuming that water with identical characteristics to the surface layer was laterally advected. Model grid spacing was designed to be consistent with the DMS and DMSP sampling interval and was thus concentrated in the upper 40 m ($\sim$ every 5 m) to resolve surface processes, with spacing below this depth increasing gradually to approximately 20 m at the bottom of the model domain. The model was initialized with observed conditions corresponding to 1 January 1992 (temperature = 19.5 °C, salinity = 36.6 psu, mixed layer depth = 140 m) and bottom boundary conditions (400 m) were set to 18.0 °C and 36.49 psu.

[25] DMS cycling was computed in a 1-D offline transport model using archived T, S, and K_z from the KPP simulation. The sulfur model was solved forward in time using a stiff ODE solver with an adaptive time step (average time step < 4 hours). Inverse modeling techniques including the Nelder-Mead simplex algorithm [*Nelder and Mead*, 1964] were used to optimize the model results to the *Dacey et al.* [1998] twice monthly vertical profiles of DMS. The inverse fitting was carried out to adjust a set of biological parameters (Table 2) using unconstrained linear optimization to minimize the sum of squared error between the measured and modeled DMS concentrations in the upper 140 m (the maximum depth of DMS concentration sampling).

4. Results and Discussion

4.1. Physical Environment

[26] The physical model accurately reproduced the seasonal temperature cycle at BATS (Figure 2). The simulated mixed layer depths reasonably recreated the seasonal structure of mixing although summertime depths were underestimated by $\sim$10% (Figure 2c). The 1-D physical model does not parameterize eddies, so it is not surprising that it does not capture the variability in mixing depth due to their passage (see February 1994) [*Doney*, 1996]. Overall, the seasonal dynamics are sufficiently resolved to experiment with DMS cycling submodels.

4.2. DMS Distribution

[27] Figure 5 shows contours of the observed *Dacey et al.* [1998] DMS concentration data and the DMS concentrations simulated using the KPP physical model coupled to the light driven DMS cycling submodel (r^2 = 0.71 for model-data comparison). The simulated DMS distribution accurately depicts many of the salient features of the observed DMS distribution in the Sargasso Sea including the summertime maxima. Values are low (<1 μmol m^{-3}) and uniform with depth in the winter during deep convective mixing and gradually increase concomitant to the spring shoaling of the mixed layer (Figures 5a and 5b). Simulated DMS concentrations exhibit a high subsurface maximum (5–7 μmol m^{-3}) directly below the seasonal mixed layer during the summer stratified period. The profile is also characterized by a general decrease towards the surface during this time. Model-data concentration differences (Figure 5c) indicate that during most periods of the year, simulated DMS concentrations are within $\pm$1 μmol m^{-3} of the observed values (Figure 5c). Relatively larger anomalies are associated with patchiness in the DMS distribution, potentially due to strong wind events that can substantially decrease DMS inventories or the passage of unresolved eddies.

[28] Summertime profiles indicate that the depth of the mid water column buildup, the summer paradox, is accurately depicted, although the absolute magnitude is underestimated by as much as 2 μmol m^{-3}. During springtime, modeled DMS concentrations start to build-up earlier in the year as compared to observations. Because DMS and DMSP cycling is so rapid, slight perturbations to rate

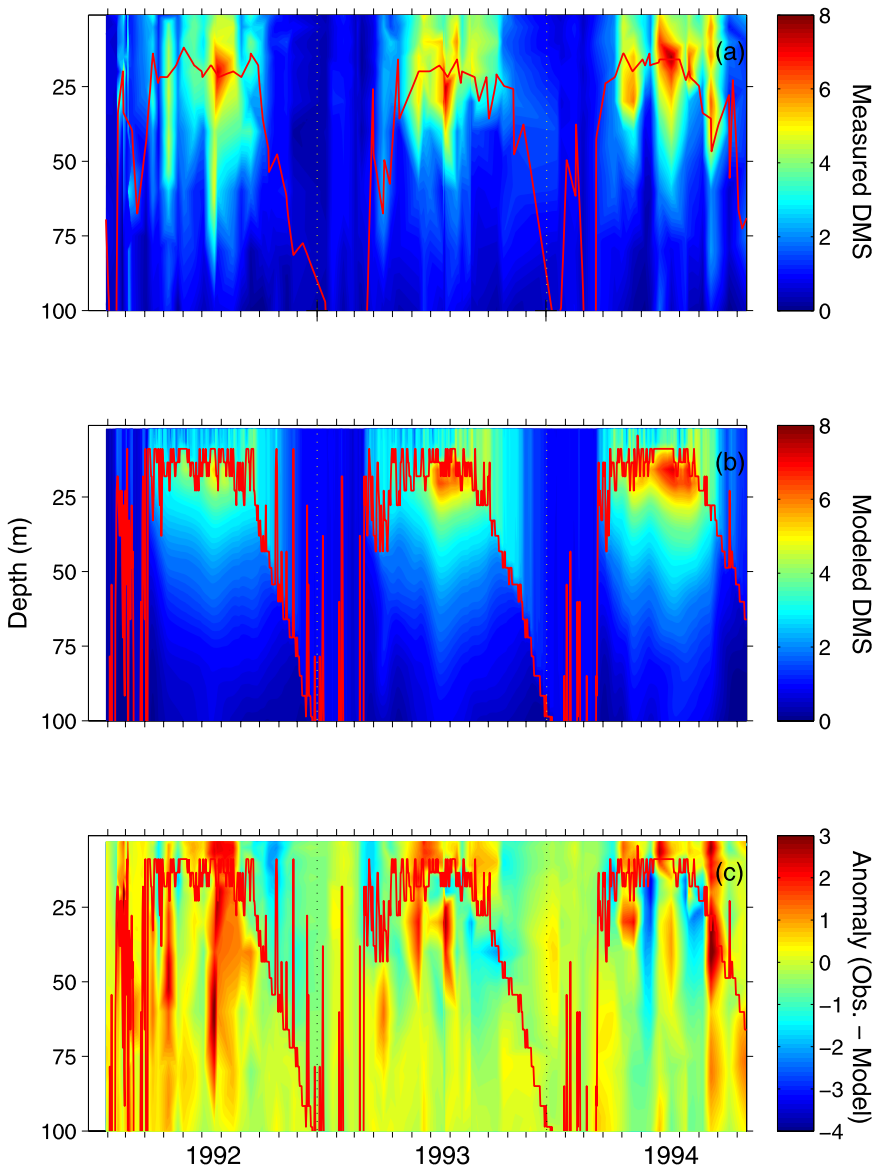

Figure 5. Contour plots of (a) the *Dacey et al.* [1998] 1992–1994 measured DMS distribution (μmol m^{-3}), (b) the best fit simulated DMS distribution (μmol m^{-3}), and (c) the absolute difference between these distributions (μmol m^{-3}, measured-modeled). The red line represents the mixed layer depth (m) in all panels, and the vertical dotted lines represent 1 January of each year.

processes can quickly result in large changes in in situ concentrations. It is likely that this difference was a result of a process not accurately reproduced in the current model such as an overemphasis of, or variability in, the role of visible light saturation for phytoplankton. This is not surprising as many of the input data sets were derived from reanalysis data or bimonthly data sets.

[29] Because atmospheric ventilation is primarily forced by surface DMS concentrations, a great deal of effort has been expended to quantify and map these distributions. While the current DMS model was optimized to recreate the vertical structure of seasonal DMS cycling, it accurately simulates the seasonal cycle and absolute concentrations of surface DMS (r^2 = 0.61) (Figure 6a). Simulated and modeled mean mixed layer stocks are also in good agreement (Figure 6b). Unlike the measured data set, however, simulated mixed layer integrated DMS stocks do display a slight seasonality, peaking in the winter (Figure 6c).

4.3. Rate Process Assessments

[30] As with any numerical simulation it is important to examine the fit parameters and modeled rate processes to assess the underlying assumptions and limitations of the model structure. In this section, simulated DMS production and loss rates are assessed in relationship to published and theorized mechanisms to assess validity. In addition, sensitivity analyses are carried out which involve (1) varying each parameter by ±50%, (2) utilizing literature DMSPd concentrations [*Dacey et al.*, 1998], and (3) utilizing seasonal means for light inputs and assessing the resulting impact on surface DMS concentrations.

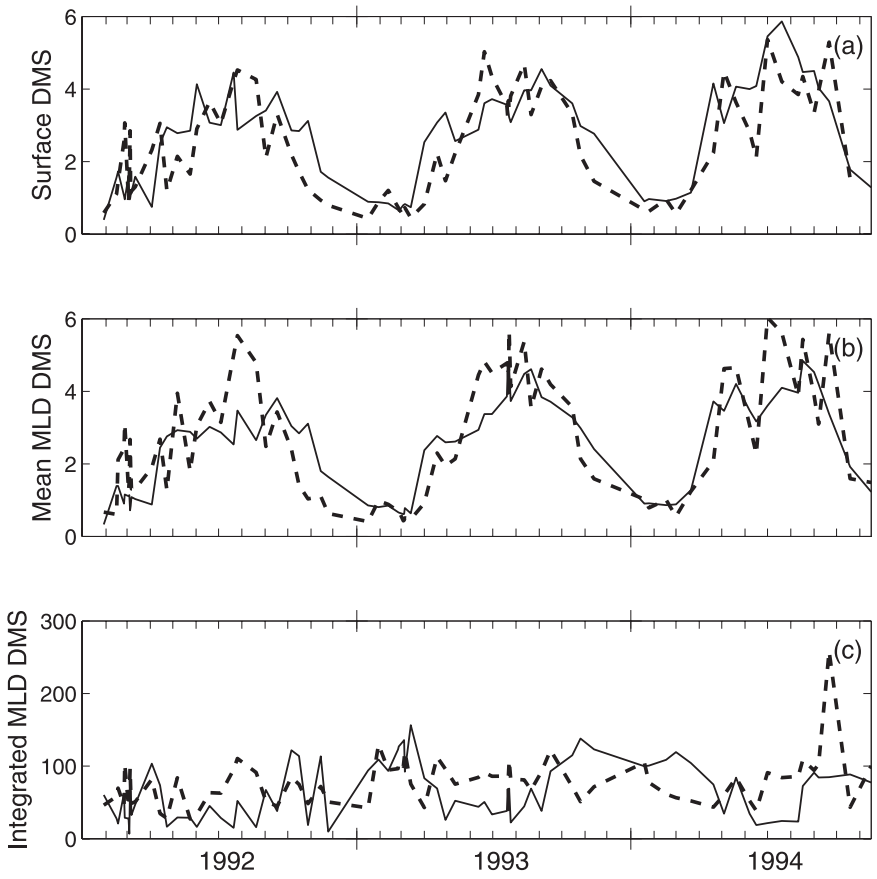

Figure 6. Temporal comparison between measured and modeled (a) surface DMS concentrations (μmol m^{-3}), (b) mean mixed layer DMS concentrations (μmol m^{-3}), and (c) mixed layer integrated DMS concentrations (μmol m^{-2}). Data are only presented for the days on which in situ DMS samples were taken and are interpolated linearly between observations. In all panels the solid line corresponds to model output, while the dashed line is observations.

4.3.1. DMS Photolysis

[31] Simulated DMS photolysis rates were not optimized and vary seasonally peaking in the summertime associated with higher temperatures, higher DMS concentrations, and shallower mixed layer depths. Surface photolysis rates range from less than 0.2 μmol m^{-3} d^{-1} in the winter to greater than 0.9 μmol m^{-3} d^{-1} in the summer (Figure 7a). DMS photolysis rates range from $\sim$0 μmol m^{-3} d^{-1} at depths below the euphotic zone to as large as 0.92 μmol m^{-3} d^{-1} (mean over the upper 140 m = 0.12 $\pm$ 0.30 μmol m^{-3} d^{-1}). Integrated mixed layer rates are consistent in magnitude and seasonal pattern with those observed by *Toole et al.* [2003] ranging from <1 μmol m^{-2} d^{-1} in the winter to greater than 12 μmol m^{-2} d^{-1} in the summer (data not shown). As simulated sea surface DMS concentrations are slightly lower than observed concentrations, the absolute magnitude of modeled mixed layer photolysis is also lower as it is a first-order rate process [e.g., *Kieber et al.*, 1996].

4.3.2. Bacterial DMS Consumption

[32] Bacterial DMS consumption rates (equation (5)) included a prescribed dark rate constant of 0.25 d^{-1}. Simulated surface consumption rates were extremely low and peaked in the wintertime (Figure 7b). At a depth of 25 m, consumption rates increased dramatically to as large as 0.64 μmol m^{-3} d^{-1} due to higher DMS concentration during the summer months and the near 100% attenuation of UV-B radiation. At depths of 100 m the consumption rates are fairly uniform with season ranging from 0.05–0.21 μmol m^{-3} d^{-1}. These values are consistent with other studies that have observed a large range of bacterial DMS consumption rates at shallow depths ranging up to $\sim$4 μmol m^{-3} d^{-1}. In the Sargasso Sea, however, consistent with our model results, particularly low values have been observed at depth (<0.5 μmol m^{-3} d^{-1}) with higher values up to 0.8 μmol m^{-3} d^{-1} observed at the summertime DMS concentration maximum [e.g., *Kieber et al.*, 1996; *Ledyard and Dacey*, 1996; *Simó and Pedrós-Alió*, 1999b; *Jodwalis et al.*, 2000; *Levasseur et al.*, 2004; *del Valle et al.*, 2007]. While mean mixed layer bacterial consumption rates are low throughout the year, they are the dominant DMS loss process during the winter and at depth.

[33] While previous studies have shown that for a particular species of bacteria, DMS consumption is linearly related to DMS concentration and temperature [*Kiene and Service*, 1991], there are seasonal changes in bacterial community structure related to DOM quality which will impact DMS consumption. *Carlson et al.* [2002] demonstrated that under experimental conditions, the bacterial community structure in the Sargasso Sea rapidly responds to changes in DOM quality. In the summertime, DOM

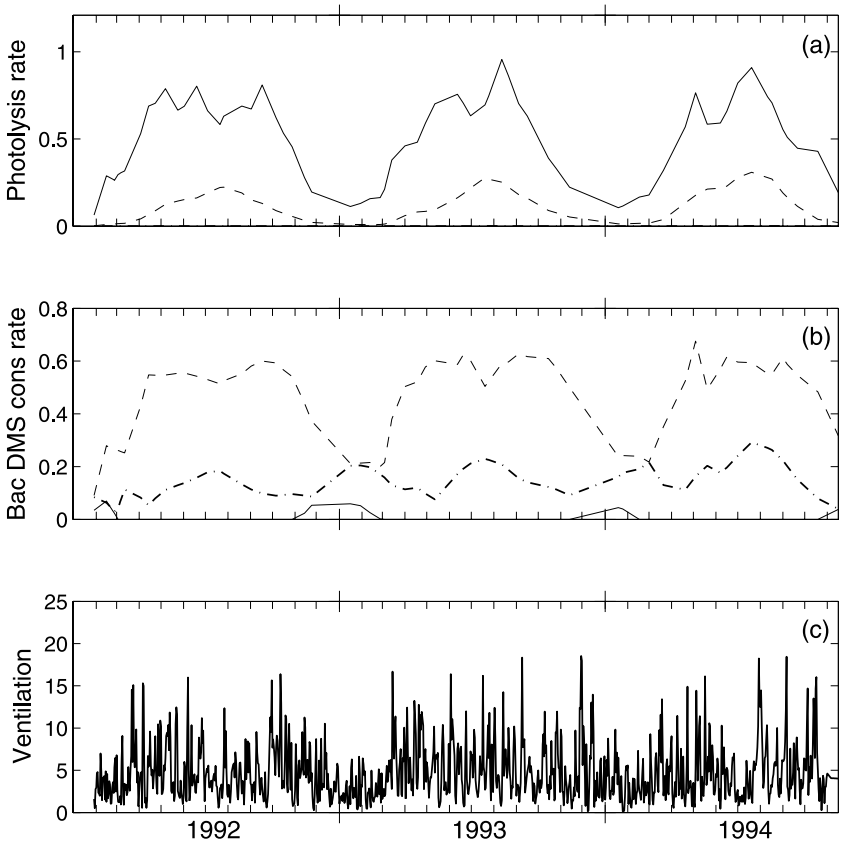

Figure 7. Simulated DMS loss rates as a function of time: (a) photolysis (μmol m^{-3} d^{-1}), (b) bacterial DMS consumption (μmol m^{-3} d^{-1}), and (c) atmospheric DMS ventilation (μmol m^{-2} d^{-1}). In Figures 7a and 7b the solid line is surface, the dashed line is 25 m, and the dash-dot line is 100 m.

resistant to bacterial consumption builds up concomitant to an increase in bacterial abundance and productivity implying that the bacteria are rapidly turning over a labile source of carbon and sulfur. DMS has been shown to be a nonideal substrate for carbon incorporation suggesting that it is consumed only when other more labile substrates are not available [*Zubkov et al.*, 2002]. The relationship between DOM succession and bacterial consumption shifts is an alternative mechanism not modeled presently.

4.3.3. DMS Sea-Air Flux

[34] Similar to photolysis, the parameterization for atmospheric ventilation did not involve optimized coefficients and was constrained following equation (12). DMS sea-air flux ranged from ~5 μmol m^{-2} d^{-1} in the winter as a result of lower surface DMS concentrations to synoptic peak values greater than 15 μmol m^{-2} d^{-1} in the summer (Figure 7c). Although peak wind speeds are lower in the summertime, atmospheric ventilation is greater as a result of the concomitant higher DMS concentrations and sea surface temperatures. The mean rate of change in DMS averaged over the mixed layer was -0.23 ± 0.26 μmol m^{-3} d^{-1}. Although the maximum rate (-1.81 μmol m^{-3} d^{-1}) and mean value are greater than those for photolysis, the variability tends to be synoptic with seasonally, ventilation processes having a smaller impact on the time/space variability of DMS. DMS photolysis, sea-air flux, and bacterial consumption processes all peak in the summertime, however, exacerbating the DMS summer paradox.

4.3.4. Bacterial DMS Production From DMSPd

[35] Bacterial DMS production rates were derived as a function of a single parameter that was optimized during model calibration (c_2): the conversion factor between cell count normalized bacterial production and DMSPd consumption. The conversion parameter for bacterial production c_2 was optimized to 12.7 10^8 cells mg C^{-1}. Based on this optimized parameter, bacterial DMSPd consumption rates ranged up to 4 μmol DMSPd m^{-3} d^{-1} which is within the large span of literature values that range from <2–51 μmol m^{-3} d^{-1} (data not shown) [e.g., *Ledyard and Dacey*, 1996; *Simó and Pedrós-Alió*, 1999b; *Kiene and Linn*, 2000a]. Taking into account the difficulty associated with choosing the correct scaling factors for the conversion of leucine uptake rates to carbon growth, bacterial growth efficiency, and the DMSPd consumption to assimilation ratio, this factor can be cautiously compared to literature results. The Sargasso Sea is characterized by some of the lowest observed bacterial growth rates anywhere [*Carlson et al.*, 1996]. Assuming a conservative bacterial growth rate efficiency (0.05–0.10), and using an average bacterial abundance (5.51 x 10^8 cells m^{-3}) and productivity (0.359 mg C m^{-3} d^{-1}) for the upper 100 m, the DMSPd to bacterial production conversion factor equates to DMSPd consumption supporting 3.8–7.6% of bacterial carbon demand. This is within literature values, which range from ~1–20% [e.g., *Kiene and Linn*, 2000a; *Simó et al.*, 2002], suggesting that the simulated rates are reasonable.

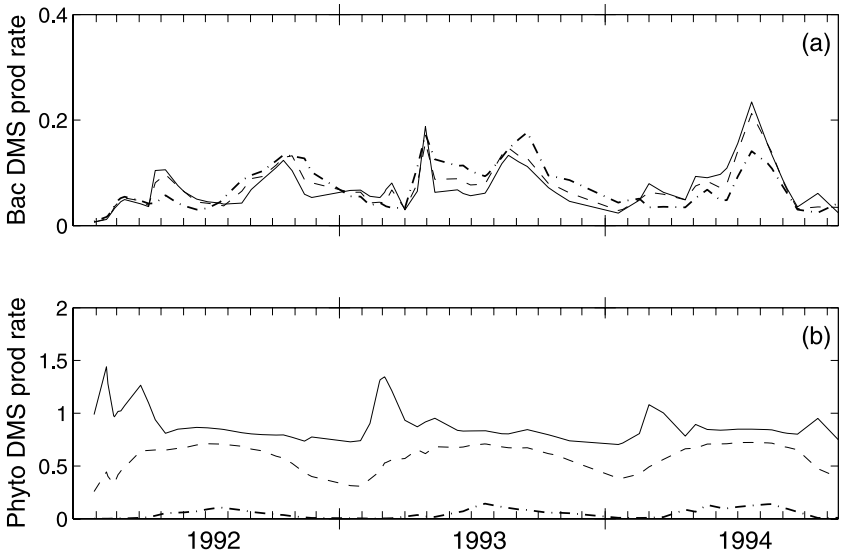

Figure 8. Simulated DMS production rates as a function of time (a) bacterial DMS production from DMSPd consumption assuming a 10% yield (μmol m^{-3} d^{-1}) and (b) phytoplankton DMS release into the water column (μmol m^{-3} d^{-1}). In Figures 8a and 8b the solid line is surface, the dashed line is 25 m, and the dash-dot line is 100 m.

[36] The combination of this optimized parameter and a 10% DMS yield via equation (6) yielded bacterial DMS production rates that ranged from 0.01–0.24 μmol m^{-3} d^{-1} at the surface, characterized by slightly increased rates in the summer at all depths (Figure 8a). In the model simulation, bacterial production and bacterial consumption of DMS at 100 m are both ~0.1 μmol m^{-3} d^{-1} suggesting a close balance between bacterial production and loss processes in the absence of UV radiation. In the fall, bacterial DMS consumption rates greatly exceed bacterial DMS production rates indicating a net loss of DMS. This is reflected in the gradual decrease in concentration during this period. During deep wintertime mixing, bacterial DMS production and loss terms are also nearly identical suggesting that the bacterial processes are closer to steady state.

4.3.5. Phytoplankton DMS Production

[37] Simulated phytoplankton DMS production rates depended on four optimized parameters: (1) the scaling factor for the PAR saturation irradiance overflow mechanism (c_3), (2) the BWF constant (c_4), (3) the BWF slope (c_5), and (4) the maximum rate of intracellular DMS release due to UVR-induced stress (c_6). DMS production was in part modeled as the difference between saturated primary production rates (equation (8a)) and estimated unsaturated rates using the average P-E slope at irradiance fluxes less than saturation. This difference was scaled by an optimized primary production normalized DMS production rate (c_3, 0.0045 μmol DMS mg C^{-1}) and measured primary production rates. Modeled I_k values closely match those derived from the BATS core primary production data set (5.43 ± 0.95 modeled versus 5.43 ± 4.47 Ein m^{-2} d^{-1} [see *Siegel et al.*, 2001]). The simulated PAR-induced DMS production rates peak in the spring associated with increasing levels of PAR, shoaling of the mixed layer depth (and thus more time at saturating levels so more excess energy), and the primary production peak. This is also consistent with the study of *Sunda et al.* [2002] which observed that under increased PAR radiation, a small but significant increase in intracellular DMS and DMSPp was observed.

[38] Phytoplankton DMS release rates were also modeled as a function of UVR-induced stress via an optimized biological weighting function. This optimized biological weighting function is greater and weights longer wavelengths more heavily than those determined for photosynthesis by *Neale et al.* [1998a] as a result of a smaller optimized exponential constant (c_4, 4.66 vs. 25.2) and a smaller exponential slope (c_5, 0.034 vs. 0.107). This variation is not unexpected though, and the optimized BWF is within a reasonable range as considerable variability has been observed in BWFs as a result of location, species composition, and light history [see *Day and Neale*, 2002]. The BWF was combined with vertical profiles of wavelength resolved UVR following equation (10) to produce an index of UV stress. This dimensionless index ranged from 0 to 1, with mean mixed layer values of >0.9 in the summer and <0.1 in the winter (data not shown). It should be noted that because the calculation of $E_{inh}(z)$ integrates across wavelength, similar values of the UVR stress index can be simulated with varying c_4 and c_5 values. The slope modulates the relative weightings and thus depth horizon over which the UVR-stress induced release of DMS is observed however, suggesting that it occurs relatively deep in the water column. The optimized maximum rate of phytoplankton DMS release due to UVR stress (resulting from direct exudation, zooplankton grazing, cell lysis) was 0.77 μmol DMS m^{-3} d^{-1}. When this factor is scaled to the UVR stress index, phytoplankton DMS release ranged from 0.68–0.74 μmol m^{-3} d^{-1} at the surface, 0.15–0.68 μmol m^{-3} d^{-1} at 25 m, and decreased with depth to approximately zero at depths below significant penetration of UVR (Figure 8). Total phytoplankton release (PAR overflow + UVR stress) was as large as 1.55 μmol m^{-3} d^{-1} in the upper 10 m during the annual spring phytoplankton bloom. At all other depths, modeled phytoplankton DMS release rates

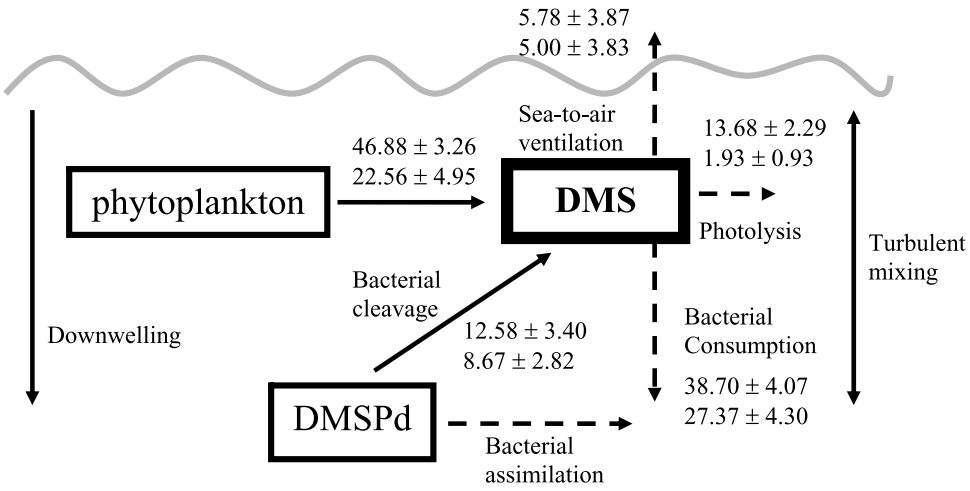

Figure 9. Simulated mean integrated upper 140 m fluxes for the primary DMS biogeochemical cycling processes ± standard deviation (μmol m^{-2} d^{-1}). The upper value for each process corresponds to summer (June–August), and the lower value corresponds to winter (December–January).

peak in the summer concomitant to the observed DMS maxima and are of sufficient magnitude to balance the loss processes and produce the summer paradox (Figure 8). During the annual spring bloom, the PAR induced overflow mechanism accounted for upwards of 50% of the observed DMS release at shallow depths. Throughout the rest of the year, and at depths >60 m in the spring, modeled phytoplankton DMS release was dominated by UVR-induced stress effects accounting for upwards of 90% of the total. Phytoplankton release rates are at an annual minimum in winter due to lower UVR and PAR fluxes and deeper mixing conditions.

[39] Utilizing estimated summertime cell size for eukaryotic phytoplankton and coccolithophorids (2 μm and 7 μm respectively) and cell density (~20 cells mL^{-1} and 3 cells mL^{-1} respectively) for the Sargasso Sea [see *DuRand et al.*, 2001] suggests that the maximum surface production of DMS is equivalent to 0.0025 fmol DMS μm^{-3} cell volume d^{-1}. In the wintertime this value decreases to 0.0013 fmol DMS μm^{-3} cell volume d^{-1}. These values take into account not just direct phytoplankton exudation of DMS but also zooplankton grazing and cell lysis due to viruses and natural mortality, processes which are unlikely to be directly impacted by UVR or PAR fluxes or exposure dose. It is difficult to quantitatively evaluate the role of microzooplankton grazing however. Literature estimates suggest anywhere from 65 to 75% of ingested DMSPp is released as DMSPd and DMS [e.g., *Burkill et al.*, 2002; *Simó et al.*, 2002] to a lack of statistical relationship between DMS and grazing rates [e.g., *Cantin et al.*, 1996]. Many past successful models have parameterized grazing ingestion rates as a constant percentage across season. The available field data from the BATS site supports this, suggesting that variations in grazing rates, and thus DMS production, are not responsible for the modeled phytoplankton DMS production. While seasonal phytoplankton community succession, variations in biomass, or other factors such as direct exudation or cell lysis can not be specifically isolated as the mediating phytoplankton mechanism, the success of the current simulation suggests that physical and optical variations drive phytoplankton DMS production in this region. Future efforts with fully resolved ecosystem models are necessary to determine the exact phytoplankton production mechanism(s) responsible for the increased summertime DMS production.

4.4. Seasonal Patterns of DMS Rate Processes

[40] Figure 9 shows mean integrated upper 140 m DMS fluxes for summer (June–August) and winter (December–January) time periods for the primary DMS rate processes. Not unexpectedly, surface photolysis rates peak in the summer (and attenuate more slowly) and are at a minimum in the winter due to lower UVR availability, lower temperatures, and lower in situ DMS concentrations. While bacterial DMS consumption does show significant UVR inhibition in the upper water column during periods of strong stratification (Figures 7b and 10), when integrated over the upper 140 m, integrated values peak in the summer with a mean value of 38.7 ± 4.1 μmol m^{-2} d^{-1}. This is in large part due to the consumption rate peak at depths of 20–60 m as bacterial DMS consumption is a first order rate process. Similar to field studies [e.g., *Toole et al.*, 2006], summertime bacterial DMS consumption and photolysis rates reach an equivalence point in the upper water column at a depth of approximately 20 m. Below this depth horizon there is negligible UV-B radiation and bacterial consumption is the dominant loss process (Figure 10). Ventilation to the atmosphere shows the least amount of seasonality ranging from a mean of 5.8 ± 3.9 μmol m^{-2} d^{-1} in the summer to 5.0 ± 3.8 μmol m^{-2} d^{-1} in the winter suggesting that the increased DMS concentrations and temperatures in the summer are balanced by increased wind speeds in the wintertime. Bacterial DMS production also peaks in the summer with a mean value of 12.6 ± 3.4 μmol m^{-2} d^{-1} indicating that the net effect of bacteria on the sulfur cycle is also consumption during this time. The largest rate term is phytoplankton DMS production which varies by a factor of 2 seasonally ranging from 46.9 ± 3.3 μmol m^{-2} d^{-1} in the summer to 22.6 ± 4.9 μmol m^{-2} d^{-1} in the winter. Phytoplankton DMS production rates attenuate much less rapidly

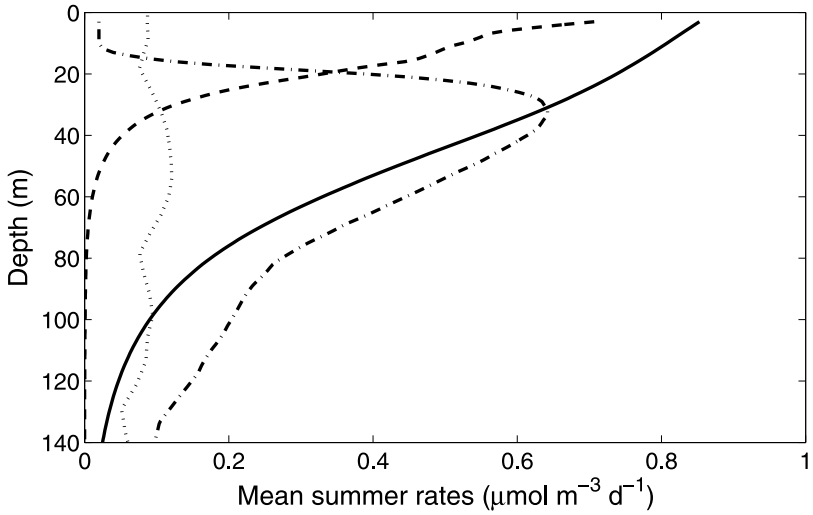

Figure 10. Simulated summertime (June–August) mean vertical profiles for the primary DMS biogeochemical cycling processes (μmol m^{-3} d^{-1}) including photolysis (dashed), bacterial consumption (dash-dot), bacterial production (dotted), and phytoplankton production (solid).

than photolysis rates due to the importance of longer UV-A and PAR wavelengths (Figure 10). Overall, while all rate processes are larger in the summer, production processes are just slightly larger (59.5 ± 4.7 μmol m^{-2} d^{-1}) and decoupled from the loss processes (58.2 ± 6.1 μmol m^{-2} d^{-1}) allowing for a slow but continual build-up of DMS, creating the DMS summer paradox. The opposite scenario occurs in the winter (31.2 ± 5.7 μmol m^{-2} d^{-1} production versus 34.3 ± 5.8 μmol m^{-2} d^{-1} loss).

4.5. Sensitivity Analysis

[41] A sensitivity analysis was carried out to assess the impact of each individual rate process on the model results (Figure 11). Each parameter was varied by ±50% relative to the optimized value, or in the case of nonoptimized processes or values (DMS yield from DMSPd consumption, dark bacterial DMS consumption rate constant, photolysis, sea-air flux), relative to the prescribed value. Even though the model was not originally optimized for sea surface concentrations, this metric was chosen for comparison because in DMS studies, the quantity of interest is often atmospheric ventilation.

[42] Varying the bacterial DMS production terms (yield and c_2) and production of DMS by phytoplankton resulting from exposure to PAR above saturating levels (c_3) by ±50% had a relatively small effect on the relative difference between the newly optimized concentrations and the best-fit model run suggesting that the model is relatively insensitive to these parameters (Figure 11). For these simulations, and all of those discussed below, the difference between the sensitivity runs and the best-fit simulation and the difference between the sensitivity runs and the observed concentrations were qualitatively similar (data not shown). The model is moderately sensitive to bacterial DMS consumption rates (k_{dark} and c_1). Simulated DMS output is the most sensitive to the surface oriented loss processes of flux and photolysis and parameters which constrain the effect of UVR on DMS release by phytoplankton (c_4, c_5, and c_6). Although the relative difference changed significantly, varying the maximum phytoplankton UVR-induced release rate had little effect on r^2 values, indicating that changing this factor imparts a systematic bias on surface DMS concentrations. Decreasing the BWF constant (c_4) by 50% and increasing the BWF slope (c_5) by 50% had an enormous impact on the retrieved DMS sea surface concentrations however (r^2 = 0.14 and r^2 = 0.01 respectively). Following equation (9), the BWF slope and constant determine the weighted phyto-

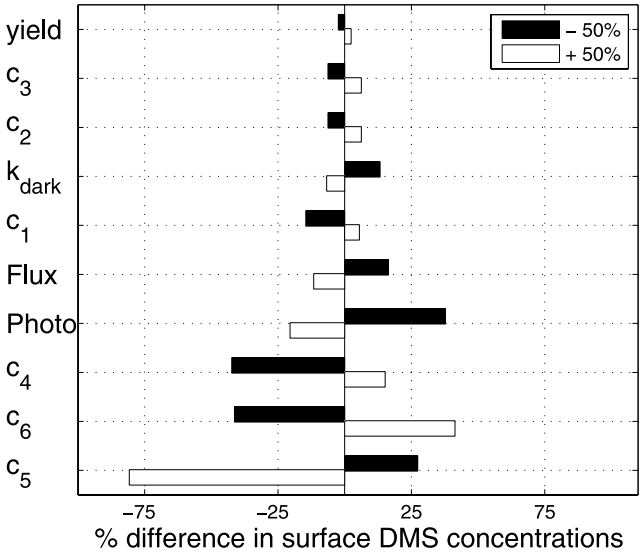

Figure 11. Results of the model sensitivity analysis. Each optimized parameter, model coefficient, or process (in the case of ventilation and photolysis) was modified by + (white bars) or − (solid bars) 50%, and the percentage difference from optimized surface DMS concentrations was calculated. The parameters are arranged in order of increasing sensitivity.

plankton response to UVR and the depth horizon over which DMS release will occur. A decrease in the biological weighting function constant (c_4), coupled with a shift towards wavelengths associated with lower incident fluxes (increase c_5), greatly decreases the magnitude of modeled phytoplankton DMS release and restricts the depth horizon over which the release occurs, resulting in low r^2 values and high relative differences. An opposite trend is seen when the BWF constant is increased by 50% and the BWF slope is decreased by 50%. The higher BWF constant and shift towards longer wavelengths leads to more modeled UVR-induced phytoplankton DMS release over a deeper depth horizon and thus an overestimation of surface DMS concentrations. This sensitivity study suggests that future work needs to specifically focus on resolving the wavelength resolved response of phytoplankton to UVR exposure.

[43] To assess the effects of applying a constant DMSPd concentration for model optimization two sensitivity runs were carried out: (1) the model was run forward with the originally optimized coefficients (Table 2) but the *Dacey et al.* [1998] DMSPd concentrations and (2) the model was reoptimized with the *Dacey et al.* [1998] DMSPd concentrations as input (rather than the constant 1 nM). In the first case, there was a slightly diminished model-measurement fit (r^2 = 0.61 versus 0.71 for the optimized case). This is not surprising as the sensitivity analysis demonstrates that the model is not overly sensitive to either the yield term or c_2, and thus the DMSPd concentration, as they are not truly independent. The DMS maxima co-occurred with large DMSPd concentrations, however, and the vertical structure was also impacted with peak DMS concentrations extending to the surface and much deeper into the water column than observed. When the model was reoptimized with *Dacey et al.* [1998] DMSPd concentrations as input a significantly damped seasonal cycle was observed with higher winter (>1 nM) and lower summer (<4 nM) DMS concentrations at the surface (data not shown). Simulated DMS concentrations peaked earlier and exhibited a lower subsurface maximum relative to the observations and the optimized model simulation (4–5 versus 6–8 μmol m^{-3}). The optimized factors for the biological weighting function slope and constant (c_4 and c_5) and bacterial DMS consumption remained largely unchanged. In contrast to this, the normalized bacterial carbon production to DMSPd consumption conversion factor (c_2) is reduced 9-fold due not only to the significantly larger DMSPd concentrations, but the noisiness in space and time. The maximum rate of phytoplankton DMS release from UVR induced stress increased to account for the significantly reduced DMS yield from DMSPd consumption. In both sensitivity simulations, better model-data agreement was found using the constant value for DMSPd concentrations but clearly this value needs to be verified with field observations. These results suggest that either the original DMSPd time series data set is subject to methodological biases and noise or that the model structure is not complex enough to capture variations in DMSPd consumption due to unresolved changes in bacterial sulfur demands.

4.6. Mixing Versus UVR Availability

[44] Past studies have suggested that phytoplankton up-regulate their antioxidant protection systems in response to oxidative stress. Assuming that DMSP, DMS, and their derivatives do form the basis for such a protection system, and that UVR exposure is the primary oxidative stressor at BATS, it is critical to assess whether it is the actual seasonal variation in surface UVR availability *or* the time-varying exposure pattern which convolves the seasonal UVR cycle with the seasonal cycle of mixing and CDOM absorption, that regulates the increased summertime production rates and concentrations. To assess this, the model was run forward using the optimized coefficients (Table 2), and each DMS and DMSP cycling process was altered (individually or in combination) to be a function of mean downwelling light flux, rather than the temporally resolved flux, while allowing mixing and temperature profiles to retain their seasonality. When a process was modified, mean values for the three year time series for all light dependent or light altering properties (e.g., surface downwelling irradiance, diffuse attenuation coefficients, absorption by CDOM, saturation irradiance) were utilized.

[45] As compared to the optimized DMS distribution, RMS errors in the upper 140 m increased by <1% when using annual mean values for the light parameters necessary to describe bacterial DMS production and the PAR saturation overflow mechanism. These rate processes are primarily forced by measured productivity rates from the BATS site, with a relatively smaller dependence on light. DMS photolysis, bacterial DMS consumption, phytoplankton DMS release resulting from UVR stress only, and total phytoplankton DMS release resulting from UVR and PAR stress each impacted RMS errors fairly similarly (10.1, 13.4, 11.3 and 11.6 % respectively). The most striking changes in RMS error resulted from using the mean UVR values for the calculation of all loss processes (18.8 % increase) and when mean UVR was used for all calculations (35.6 % increase). To assure that this is not simply a residual of using the originally optimized coefficients the model was reoptimized using mean surface UVR and PAR flux, attenuation coefficients, and absorption by CDOM as inputs to all model equations. This produced a diminished model-measurement fit (r^2 = 0.33) and a significantly damped seasonal cycle with higher winter concentrations and lower summer concentrations. In addition, the optimized simulation produced significantly lower maximum summer concentration (~3.6 nM, data not shown), was unable to recreate the summertime DMS subsurface concentration peak, and had no depth structure within the upper mixed layer. This indicates that seasonal changes in the water column structure associated with mixing are not enough to create the large observed seasonal change in DMS concentration distribution. In contrast to mixing however, seasonal UVR dose in the upper-water column ranges over several orders of magnitude due to higher UVR fluxes (~2–3 times greater in the summertime [*Lubin et al.*, 1998]) occurring concurrently with significantly shallower mixed layers and significantly lower attenuation coefficients (Figure 2d). This verifies that it is the time-varying pattern of UVR dose on the phytoplankton population that determines their oxidative stress and ultimately their release of DMS to the water column. Our current results suggest that unlike past modeling efforts, mixed layer depth and wavelength resolved surface light availability and penetration into the water column need to be incorporated to

increase our ability to simulate the seasonal cycle of DMS in this subtropical gyre region.

5. Conclusion

[46] This work represents the first diagnostic model of DMS cycling to describe the vertical distribution of DMS in an open ocean region explicitly incorporating the effects of wavelength resolved UVR. The model was formulated using a 'minimalist approach' indicating that only DMS was simulated, the sulfur cycling model was not embedded in an ecosystem model, and concurrently sampled oceanographic observations were utilized wherever possible. This basic model was able to capture the DMS temporal and vertical structure variability, including the summertime midwater-column peak, displayed in the *Dacey et al.* [1998] DMS data set. While seasonal phytoplankton community succession or variations in biomass can not be explicitly ruled out, the success of the current simulation suggests that physical and optical variations are capable of driving DMS biogeochemical cycling in this region. Sensitivity analyses indicate that the model is the most sensitive to the surface oriented loss processes of ventilation to the atmosphere and photolysis and parameters which constrain the effect of UVR on DMS release by phytoplankton. Correspondingly, a comparison of the distribution of rate processes indicates that the principal processes mediating the DMS summer paradox are phytoplankton DMS release increasing in the summer, towards the surface as a result of UVR and PAR stress (due to high daily exposure resulting from high flux and strong stratification) superimposed upon, but extending deeper into the water column than, photolysis and sea-to-air flux. This is consistent with several modeling and field studies which have highlighted the emerging evidence for the importance of DMS production by phytoplankton [e.g., *Toole and Siegel*, 2004; *Toole et al.*, 2006; *Bailey et al.*, 2008; *Vallina et al.*, 2008].

[47] The model simulations also highlight the importance of including wavelength resolved UV and visible solar radiation as well as state variables which impact their vertical attenuation (i.e., absorption by CDOM, chlorophyll). This is crucial given that different DMS cycling processes are differentially impacted by various regions of the solar spectrum. For example, photolysis action spectra in the Sargasso Sea peak at approximately 320–330 nm [*Toole et al.*, 2003] whereas phytoplankton DMS production can increase substantially due to UV-A exposure in the absence of UV-B [*Sunda et al.*, 2002]. These differences suggest corresponding depth horizons for the various processes that will not be adequately reproduced without accurate wavelength resolved flux and attenuation values. The weaknesses of the current model simulation also identify key candidates for future field studies including the DMS yield from bacterial DMSPd consumption, DMSPd concentration variability using emerging techniques, and the kinetics of inhibition and recovery associated with the marine sulfur cycle. More research is necessary to isolate the mechanisms and functionalities of these parameters so they can be modeled more rigorously in future efforts. Until recently intracellular sulfur concentrations were considered relatively static within certain species dictated bounds and production and release rates were measured in the laboratory with stressors maintained at artificially low levels. Our model highlights the need to (1) consider intracellular DMS and DMSP production as dynamic quantities and (2) unlike past modeling efforts, incorporate mixed layer depth and surface light availability and penetration to increase our ability to simulate the seasonal cycle of DMS in this subtropical gyre region. A key first step is to incorporate wavelength resolved UV and visible radiation and its effect on chemical and biological cycling processes into future sulfur biogeochemical models.

[48] **Acknowledgments.** This work was supported by NASA under an Earth System Science Fellowship, a WHOI Ocean and Climate Change Institute Postdoctoral scholarship, and NSF OCE-0525928. We are extremely grateful to John Dacey for the use of his DMS and DMSP time series data sets. The authors acknowledge Scott Elliott and two anonymous reviewers for their assistance with the development of this manuscript.

References

Anderson, T. R., S. A. Spall, A. Yool, P. Cipollini, P. G. Challenor, and M. J. R. Fasham (2001), Global fields of sea surface dimethylsulfide predicted from chlorophyll, nutrients, and light, *J. Mar. Syst.*, *30*, 1–20.

Andreae, M. O., and P. J. Crutzen (1997), Atmospheric aerosols: biogeochemical sources and role in atmospheric chemistry, *Science*, *276*, 1052–1058.

Archer, S. D., F. J. Gilbert, P. D. Nightingale, M. V. Zubkov, A. H. Taylor, G. C. Smith, and P. H. Burkill (2002), Transformation of dimethylsulphoniopropionate to dimethyl sulphide during summer in the North Sea with an examination of key processes via a modelling approach, *Limnol. Oceanogr.*, *49*, 3067–3101.

Aumont, O., S. Belviso, and P. Monfray (2002), Dimethylsulfoniopropionate (DMSP) and dimethylsulfide (DMS) sea surface distributions simulated from a global three-dimensional ocean carbon cycle model, *J. Geophys. Res.*, *107*(C4), 3029, doi:10.1029/1999JC000111.

Austin, R. W. (1974), Inherent spectral radiance signals of the ocean surface, in *Ocean Color Analysis, SIO Tech. Ref. 74-10*, pp. 2.1–2.20, Scripps Inst. of Oceanogr., La Jolla, Calif.

Ayers, G. P., and R. W. Gillett (2000), DMS and its oxidation products in the remote marine atmosphere: implications for climate and atmospheric chemistry, *J. Sea Res.*, *43*, 275–286.

Ayers, G. P., and J. L. Gras (1991), Seasonal relationship between cloud condensation nuclei and aerosol methanesulphonate in marine air, *Nature*, *353*, 834–835.

Ayers, G. P., J. P. Ivey, and R. W. Gillett (1991), Coherence between seasonal cycles of dimethyl sulphide, methanesulphonate and sulphate in marine air, *Nature*, *349*, 404–406.

Bailey, K., D. A. Toole, B. W. Blomquist, R. G. Najjar, B. J. Huebert, D. J. Kieber, R. Kiene, P. A. Matrai, G. R. Westby, and D. A. del Valle (2008), Diagnosis of dimethylsulfide production in Sargasso Sea eddies, *Deep Sea Res.*, in press.

Belviso, S., et al. (2004a), Comparison of global climatological maps sea surface dimethyl sulfide, *Global Biogeochem. Cycles*, *18*, GB3013, doi:10.1029/2003GB002193.

Belviso, S., C. Moulin, L. Bopp, and J. Stefels (2004b), Assessment of a global climatology of oceanic dimethylsulfide (DMS) concentrations based on SeaWiFS imagery (1998–2001), *Can. J. Fish. Aquat. Sci.*, *61*, 804–816.

Boucher, N. P., and B. B. Prezelin (1996), Spectral modeling of UV inhibition of in situ Antarctic primary production using a field derived biological weighting function, *Photochem. Photobiol.*, *64*, 407–418.

Bouillon, R., and W. L. Miller (2004), Determination of apparent quantum yield spectra of DMS photo-degradation in an in situ iron-induced northeast Pacific Ocean bloom, *Geophys. Res. Lett.*, *31*, L06310, doi:10.1029/2004GL019536.

Boyd, P. W., and S. C. Doney (2002), Modeling regional responses by marine pelagic ecosystems to global climate change, *Geophys. Res. Lett.*, *29*(16), 1806, doi:10.1029/2001GL014130.

Brimblecombe, P., and D. Shooter (1986), Photo-oxidation of dimethylsulphide in aqueous solution, *Mar. Chem.*, *19*, 343–353.

Burkill, P. H., S. D. Archer, C. Robinson, P. D. Nightingale, S. B. Groom, G. A. Tarran, and M. V. Zubkov (2002), Dimethyl sulphide biogeochemistry within a coccolithophore bloom (DISCO): an overview, *Deep Sea Res.*, *49*, 2863–2885.

Cantin, G., M. Levasseur, M. Gosselin, and S. Michaud (1996), Role of zooplankton in the mesoscale distribution of surface dimethylsulfide con-

centrations in the Gulf of St Lawrence, Canada, *Mar. Ecol. Prog. Ser.*, *141*, 103–117.
Carlson, C. A., H. W. Ducklow, and T. D. Sleeter (1996), Stocks and dynamics of bacterioplankton in the northwestern Sargasso Sea, *Deep Sea Res.*, *43*, 491–515.
Carlson, C. A., S. J. Giovannoni, D. A. Hansell, S. J. Goldberg, R. Parsons, M. P. Otero, K. Vergin, and B. R. Wheeler (2002), Effect of nutrient amendments on bacterioplankton production, community structure, and DOC utilization in the northwestern Sargasso Sea, *Aquat. Microb. Ecol.*, *30*, 19–36.
Charlson, R. J., J. E. Lovelock, M. O. Andreae, and S. G. Warren (1987), Oceanic phytoplankton, atmospheric sulfur, cloud albedo and climate, *Nature*, *326*, 655–661.
Cropp, R. A., J. Norbury, A. J. Gabric, and R. D. Braddock (2004), Modeling dimethylsulfide production in the upper ocean, *Global Biogeochem. Cycles*, *18*, GB3005, doi:10.1029/2003GB002126.
Cullen, J. J., P. J. Neale, and M. P. Lesser (1992), Biological weighting function for the inhibition of phytoplankton photosynthesis by ultraviolet radiation, *Science*, *258*, 646–651.
Dacey, J. W. H., and N. V. Blough (1987), Hydrogen decomposition of dimethylsulfoniopropionate to from dimethylsulfide, *Geophys. Res. Lett.*, *14*, 1246–1249.
Dacey, J. W. H., and S. G. Wakeham (1986), Oceanic dimethylsulfide: production during zooplankton grazing on phytoplankton, *Science*, *233*, 1314–1316.
Dacey, J. W. H., F. A. Howse, A. F. Michaels, and S. G. Wakeham (1998), Temporal variability of dimethylsulfide and dimethylsulfoniopropionate in the Sargasso Sea, *Deep Sea Res.*, *45*, 2085–2104.
Day, T. A., and P. J. Neale (2002), Effects of UV-B radiation on terrestrial and aquatic primary producers, *Annu. Rev. Ecol. Syst.*, *33*, 371–396.
del Valle, D. A., D. J. Kieber, and R. P. Kiene (2007), Depth-dependent fate of biologically-consumed dimethylsulfide in the Sargasso Sea, *Mar. Chem.*, *103*, 197–208.
Doney, S. C. (1996), A synoptic atmospheric surface forcing data set and physical upper ocean model for the U. S. JGOFS Bermuda Atlantic Time-Series Study (BATS) site, *J. Geophys. Res.*, *101*, 25,615–25,634.
Doney, S. C., D. M. Glover, and R. G. Najjar (1996), A new coupled, one-dimensional biological-physical model for the upper ocean: Applications to the JGOFS Bermuda Atlantic Time-Series (BATS) site, *Deep Sea Res., Part II*, *43*(2–3), 591–624.
Doney, S. C., W. G. Large, and F. O. Bryan (1998), Surface ocean fluxes and water-mass transformation rates in the coupled NCAR Climate System Model, *J. Clim.*, *11*, 1420–1441.
DuRand, M. D., R. J. Olson, and S. W. Chisholm (2001), Phytoplankton population dynamics at the Bermuda Atlantic Time-series station in the Sargasso Sea, *Deep Sea Res.*, *48*, 1983–2004.
Gabric, A., N. Murray, L. Stone, and M. Kohl (1993), Modeling the production of dimethylsulfide during a phytoplankton bloom, *J. Geophys. Res.*, *98*, 22,805–22,816.
Gabric, A. J., R. Cropp, T. Hirst, and H. Marchant (2003), The sensitivity of dimethyl sulfide production to simulated climate change in the eastern Antarctic Southern Ocean, *Tellus, Ser. B*, *55*, 966–981.
Gordon, H. R., and A. Morel (1983), Remote assessment of ocean color for interpretation of satellite visible imagery: A review, in *Lecture Notes on Coastal and Estuarine Studies*, vol. 4, Springer, New York.
Hatton, A. D. (2002), Influence of photochemistry on the marine biogeochemical cycle of dimethylsulphide in the northern North Sea, *Deep Sea Res.*, *49*, 3039–3052.
Herndl, G. J., G. Muller-Niklas, and J. Frick (1993), Major role of ultraviolet-B in controlling bacterioplankton growth in the surface layer of the ocean, *Nature*, *361*, 717–719.
Herndl, G. J., A. Brugger, S. Hager, E. Kaiser, I. Obernosterer, B. Reitner, and D. Slezak (1997), Role of ultraviolet-B radiation on bacterioplankton and the availability of dissolved organic matter, *Plant Ecol.*, *128*, 42–51.
Huot, Y., W. H. Jeffrey, R. F. Davis, and J. J. Cullen (2000), Damage to DNA in bacterioplankton: A model of damage by ultraviolet radiation and its repair as influenced by vertical mixing, *Photochem. Photobiol.*, *72*, 62–74.
Jodwalis, C. M., R. L. Benner, and D. L. Eslinger (2000), Modeling of dimethyl sulfide ocean mixing, biological production, and sea-to-air flux for high latitudes, *J. Geophys. Res.*, *105*, 14,387–14,399.
Johansen, A. M., and J. M. Key (2006), Photoreductive dissolution of ferrihydrite by methanesulfinic acid: Evidence of a direct link between dimethylsulfide and iron-bioavailability, *Geophys. Res. Lett.*, *33*, L14818, doi:10.1029/2006GL026010.
Jones, A., D. L. Roberts, M. J. Woodage, and C. E. Johnson (2001), Indirect sulphate aerosol forcing in a climate model with an interactive sulphur cycle, *J. Geophys. Res.*, *106*, 20,293–20,310.
Karentz, D., J. E. Cleaver, and D. L. Mitchell (1991), Cell survival characteristics and molecular responses of Antarctic phytoplankton to ultraviolet-B radiation, *J. Phycol.*, *27*, 326–341.
Keller, M. D., W. K. Bellows, and R. R. L. Guillard (1989), Dimethyl sulfide production in marine phytoplankton, in *Biogenic Sulfur in the Environment*, edited by E. S. Saltzman and W. J. Cooper, pp. 167–182, Am. Chem. Soc., Washington, D. C.
Kettle, A. J., et al. (1999), A global database of sea surface dimethylsulfide (DMS) measurements and a procedure to predict sea surface DMS as a function of latitude, longitude, and month, *Global Biogeochem. Cycles*, *13*, 399–444.
Kieber, D. J., J. Jiao, R. P. Kiene, and T. S. Bates (1996), Impact of dimethylsulfide photochemistry on methyl sulfur cycling in the equatorial Pacific Ocean, *J. Geophys. Res.*, *101*, 3715–3722.
Kiene, R. P., and T. S. Bates (1990), Biological removal of dimethylsulfide from seawater, *Nature*, *345*, 702–705.
Kiene, R. P., and L. J. Linn (2000a), Distribution and turnover of dissolved DMSP and its relationship with bacterial production and dimethylsulfide in the Gulf of Mexico, *Limnol. Oceanogr.*, *45*, 849–861.
Kiene, R. P., and L. J. Linn (2000b), The fate of dissolved dimethylsulfoniopropionate (DMSP) in seawater: tracer studies using 35S-DMSP, *Geochim. Cosmochim. Acta*, *64*, 2797–2810.
Kiene, R. P., and S. K. Service (1991), Decomposition of dissolved DMSO and DMS in estuarine waters: dependence on temperature and substrate concentration, *Mar. Ecol. Prog. Ser.*, *76*, 1–11.
Kiene, R. P., and D. Slezak (2006), Low dissolved DMSP concentrations in seawater revealed by small-volume gravity filtration and dialysis sampling, *Limnol. Oceanogr. Methods*, *4*, 80–95.
Kirk, J. T. O. (1981), Estimation of the scattering coefficient using of natural waters using underwater irradiance measurements, *Aust. J. Mar. Freshwater Res.*, *32*, 333–339.
Large, W. G., J. C. McWilliams, and S. C. Doney (1994), Oceanic vertical mixing: A review and a model with a nonlocal boundary-layer parameterization, *Rev. Geophys.*, *32*, 363–403.
La Roche, A., A. F. Vezina, M. Levasseur, M. Gosselin, J. Stefels, M. D. Keller, P. A. Matrai, and R. L. J. Kwint (1999), DMSP synthesis and exudation in phytoplankton: a modeling approach, *Mar. Ecol. Prog. Ser.*, *180*, 37–49.
Le Clainche, Y., M. Levasseur, A. Vezina, J. W. H. Dacey, and F. J. Saucier (2004), Behaviour of the ocean DMS (P) pools in the Sargasso Sea viewed in a coupled physical-biogeochemical ocean model, *Can. J. Fish. Aquat. Sci.*, *61*, 788–803.
Ledyard, K. M., and J. W. H. Dacey (1996), Microbial cycling of DMSP and DMS in coastal and oligotrophic seawater, *Limnol. Oceanogr.*, *41*, 33–40.
Lefevre, M., A. Vezina, M. Levasseur, and J. W. H. Dacey (2002), A model of dimethylsulfide dynamics for the subtropical North Atlantic, *Deep Sea Res.*, *49*, 2221–2239.
Levasseur, M., M. Scarratt, S. Roy, D. Laroche, S. Michaud, G. Cantin, M. Gosselin, and A. Vezina (2004), Vertically resolved cycling of dimethylsulfoniopropionate (DMSP) and dimethylsulfide (DMS) in the Northwest Atlantic in spring, *Can. J. Fish. Aquat. Sci.*, *61*, 744–757.
Lubin, D., E. H. Jensen, and H. P. Gies (1998), Global surface ultraviolet radiation climatology from TOMS and ERBE data, *J. Geophys. Res.*, *103*, 26,061–26,091.
Malmstrom, R. R., R. P. Kiene, M. T. Cottrell, and D. L. Kirchman (2004), Contribution of SAR11 bacteria to dissolved dimethylsulfoniopropionate and amino acid uptake in the North Atlantic Ocean, *Appl. Environ. Microbiol.*, *70*, 4129–4135.
Maritorena, S., D. A. Siegel, and A. R. Peterson (2002), Optimization of a semianalytical ocean color model for global-scale applications, *Appl. Opt.*, *41*, 2705–2714.
McGillicuddy, D. J., A. R. Robinson, D. A. Siegel, H. W. Jannasch, R. Johnson, T. Dickey, J. McNeil, A. F. Michaels, and A. H. Knap (1998), Influence of mesoscale eddies on new production in the Sargasso Sea, *Nature*, *394*, 263–266.
McGillis, W. R., J. W. H. Dacey, N. M. Frew, E. J. Bock, and R. K. Nelson (2000), Water-air flux of dimethylsulfide, *J. Geophys. Res.*, *105*, 1187–1193.
Merzouk, A., et al. (2006), DMSP and DMS dynamics during a mesoscale iron fertilization experiment in the northeast Pacific, Part II. Bacterial cycling, *Deep Sea Res.*, *53*, 2370–2383.
Neale, P. J., J. J. Cullen, and R. F. Davis (1998a), Inhibition of marine photosynthesis by ultraviolet radiation: Variable sensitivity of phytoplankton in the Weddell-Scotia Confluence during the austral spring, *Limnol. Oceanogr.*, *43*, 433–448.
Neale, P. J., R. F. Davis, and J. J. Cullen (1998b), Interactive effects of ozone depletion and vertical mixing on photosynthesis of Antarctic phytoplankton, *Nature*, *392*, 585–589.

Nelder, J. A., and R. Mead (1964), A simplex method for function minimization, *Comput. J.*, *7*, 308–313.
Nelson, N. B., D. A. Siegel, and A. F. Michaels (1998), Seasonal dynamics of colored dissolved material in the Sargasso Sea, *Deep Sea Res.*, *45*, 931–957.
Nightingale, P. D., G. Malin, C. S. Law, A. J. Watson, P. S. Liss, M. I. Liddicoat, J. Boutin, and R. C. Upstill-Goddard (2000), In situ evaluation of air-sea gas exchange parameterizations using novel conservative and volatile tracers, *Global Biogeochem. Cycles*, *14*, 373–387.
Ohlmann, J. C., D. A. Siegel, and C. Gautier (1996), Ocean mixed layer radiant heating and solar penetration: a global analysis, *J. Clim.*, *9*, 2265–2280.
Pope, R. M., and E. S. Fry (1997), Absorption spectrum (380–700 nm) of pure water. 2. Integrating cavity measurements, *Appl. Opt.*, *36*, 8710–8723.
Ricchiazzi, P., S. Yang, C. Gautier, and D. Sowle (1998), SBDART: a research and teaching software tool for plane-parallel radiative transfer in the Earth's atmosphere, *Bull. Am. Meteorol. Soc.*, *79*, 2101–2114.
Rundel, R. D. (1983), Action spectra and estimation of biologically effective UV radiation, *Physiol. Plant.*, *58*, 360–366.
Saltzman, E. S., D. B. King, K. Holmen, and C. Leck (1993), Experimental determination of the diffusion coefficient of dimethylsulfide in water, *J. Geophys. Res.*, *98*, 16,481–16,486.
Schofield, O., B. M. A. Kroon, and B. B. Prezelin (1995), Impact of ultraviolet-B radiation on photosystem II activity and its relationship to the inhibition of carbon fixation rates for Antarctic ice algae communities, *J. Phycol.*, *31*, 703–715.
Siegel, D. A., and A. F. Michaels (1996), Quantification of nonalgal light attenuation in the Sargasso Sea: Implications for biogeochemistry and remote sensing, *Deep Sea Res.*, *43*, 321–345.
Siegel, D. A., A. F. Michaels, J. C. Sorensen, M. C. O'Brien, and M. A. Hammer (1995), Seasonal variability of light availability and utilization in the Sargasso Sea, *J. Geophys. Res.*, *100*, 8695–8713.
Siegel, D. A., et al. (2001), Bio-optical modeling of primary production on regional scales: the Bermuda BioOptics project, *Deep Sea Res.*, *48*, 1865–1896.
Simó, R. (2001), Production of atmospheric sulfur by oceanic plankton: biogeochemical, ecological and evolutionary links, *Trends Ecol. Evol.*, *16*, 287–294.
Simó, R., and J. Dachs (2002), Global ocean emission of dimethylsulfide predicted from biogeophysical data, *Global Biogeochem. Cycles*, *16*(4), 1018, doi:10.1029/2001GB001829.
Simó, R., and C. Pedrós-Alió (1999a), Role of vertical mixing in controlling the oceanic production of dimethyl sulphide, *Nature*, *402*, 396–399.
Simó, R., and C. Pedrós-Alió (1999b), Short-term variability in the open ocean cycle of dimethylsulfide, *Global Biogeochem. Cycles*, *13*, 1173–1181.
Simó, R., S. D. Archer, C. Pedrós-Alió, L. Gilpin, and C. E. Stelfox-Widdicombe (2002), Coupled dynamics of dimethylsulfoniopropionate and dimethylsulfide cycling and the microbial food web in surface waters of the North Atlantic, *Limnol. Oceanogr.*, *47*, 53–61.
Slezak, D., and G. J. Herndl (2003), effects of ultraviolet and visible radiation on the cellular concentrations of dimethylsulfoniopropionate (DMSO) in *Emiliania huxleyi* (strain L), *Mar. Ecol. Prog. Ser.*, *246*, 61–71.
Slezak, D., A. Brugger, and G. J. Herndl (2001), Impact of solar radiation on the biological removal of dimethylsulfoniopropionate and dimethylsulfide in marine surface waters, *Aquat. Microb. Ecol.*, *25*, 87–97.
Slezak, D., R. P. Kiene, D. A. Toole, R. Simó, and D. J. Kieber (2007), Effects of solar radiation on the fate of dissolved DMSP and conversion to DMS in seawater, *Aquat. Sci.*, *69*, 377–393, doi:10.1007/s00027-007-0896-z.
Stefels, J. (2000), Physiological aspects of the production and conversion of DMSP in marine algae and higher plants, *J. Sea Res.*, *43*, 183–197.
Stefels, J., M. Steinke, S. Turner, G. Malin, and S. Belviso (2007), Environmental constraints on the production and removal of the climatically active gas dimethylsulphide (DMS) and implications for ecosystem modeling, *Biogeochemistry*, *83*, 245–275.
Steinberg, D. K., C. A. Carlson, N. R. Bates, R. J. Johnson, A. F. Michaels, and A. H. Knap (2001), Overview of the U.S. JGOFS Bermuda Atlantic Time-series Study (BATS): a decade-scale look at ocean biology and biogeochemistry, *Deep Sea Res.*, *48*, 1405–1447.
Sunda, W., D. J. Kieber, R. P. Kiene, and S. Huntsman (2002), An antioxidant function for DMSP and DMS in marine algae, *Nature*, *418*, 317–320.
Toole, D. A., and D. A. Siegel (2004), Light-driven cycling of dimethylsulfide (DMS) in the Sargasso Sea: Closing the loop, *Geophys. Res. Lett.*, *31*, L09308, doi:10.1029/2004GL019581.
Toole, D. A., D. J. Kieber, R. P. Kiene, D. A. Siegel, and N. B. Nelson (2003), Photolysis and the dimethylsulfide (DMS) summer paradox in the Sargasso Sea, *Limnol. Oceanogr.*, *48*, 1088–1110.
Toole, D. A., D. Slezak, R. P. Kiene, D. J. Kieber, and D. A. Siegel (2006), Effects of solar radiation on dimethylsulfide cycling in the western Atlantic Ocean, *Deep Sea Res., Part I*, *53*, 136–153.
Vallina, S. M., and R. Simó (2007), Strong relationship between DMS and the solar radiation dose over the global surface ocean, *Science*, *315*, 506–508.
Vallina, S. M., R. Simó, and S. Gassó (2006), What controls CCN seasonality in the Southern Ocean? A statistical analysis based on satellite-derived chlorophyll and CCN and model-estimated OH radical and rainfall, *Global Biogeochem. Cycles*, *20*, GB1014, doi:10.1029/2005GB002597.
Vallina, S. M., R. Simó, T. R. Anderson, A. Gabric, R. Cropp, and J. M. Pacheco (2008), A dynamic model of oceanic sulfur (DMOS) applied to the Sargasso Sea: Simulating the dimethylsulfide (DMS) summer paradox, *J. Geophys. Res.*, *113*, G01009, doi:10.1029/2007JG000415.
Vila-Costa, M., D. A. del Valle, J. M. González, D. Slezak, R. P. Kiene, O. Sánchez, and R. Simó (2006a), Phylogenetic identification and metabolism of marine dimethylsulfide-consuming bacteria, *Environ. Microbiol.*, *8*, 2189–2200.
Vila-Costa, M., R. Simó, J. M. Gasol, B. Harada, D. Slezak, and R. P. Kiene (2006b), Dimethylsulfoniopropionate (DMSP) uptake by marine phytoplankton, *Science*, *314*, 652–654.
Zubkov, M. V., B. M. Fuchs, S. D. Archer, R. P. Kiene, R. Amann, and P. H. Burkill (2002), Rapid turnover of dissolved DMS and DMSP by defined bacterioplankton communities in the stratified euphotic zone of the North Sea, *Deep Sea Res.*, *49*, 3017–3038.

S. C. Doney and D. A. Toole, Marine Chemistry and Geochemistry Department, Woods Hole Oceanographic Institution, Woods Hole, MA 02543, USA. (dtoole@whoi.edu)

D. A. Siegel, Institute for Computational Earth System Science, University of California, Santa Barbara, Santa Barbara, CA 93106-3060, USA.